JCI The Journal of Clinical Investigation

Stromal heparan sulfate differentiates neuroblasts to suppress neuroblastoma growth

Erik H. Knelson, … , Stephen G. Marcus, Gerard C. Blobe

J Clin Invest. 2014;124(7):3016-3031. https://doi.org/10.1172/JCI74270.

Research Article **Oncology**

Neuroblastoma prognosis is dependent on both the differentiation state and stromal content of the tumor. Neuroblastoma tumor stroma is thought to suppress neuroblast growth via release of soluble differentiating factors. Here, we identified critical growth-limiting components of the differentiating stroma secretome and designed a potential therapeutic strategy based on their central mechanism of action. We demonstrated that expression of heparan sulfate proteoglycans (HSPGs), including TβRIII, GPC1, GPC3, SDC3, and SDC4, is low in neuroblasts and high in the Schwannian stroma. Evaluation of neuroblastoma patient microarray data revealed an association between *TGFBR3*, *GPC1*, and *SDC3* expression and improved prognosis. Treatment of neuroblastoma cell lines with soluble HSPGs promoted neuroblast differentiation via FGFR1 and ERK phosphorylation, leading to upregulation of the transcription factor inhibitor of DNA binding 1 (ID1). HSPGs also enhanced FGF2-dependent differentiation, and the anticoagulant heparin had a similar effect, leading to decreased neuroblast proliferation. Dissection of individual sulfation sites identified 2-O, 3-O-desulfated heparin (ODSH) as a differentiating agent, and treatment of orthotopic xenograft models with ODSH suppressed tumor growth and metastasis without anticoagulation. These studies support heparan sulfate signaling intermediates as prognostic and therapeutic neuroblastoma biomarkers and demonstrate that tumor stroma biology can inform the design of targeted molecular therapeutics.

Stromal heparan sulfate differentiates neuroblasts to suppress neuroblastoma growth

Erik H. Knelson,[1,2] Angela L. Gaviglio,[1] Jasmine C. Nee,[3] Mark D. Starr,[3] Andrew B. Nixon,[3] Stephen G. Marcus,[4] and Gerard C. Blobe[1,3]

[1]Department of Pharmacology and Cancer Biology, [2]Medical Scientist Training Program, and [3]Department of Medicine, Duke University Medical Center, Durham, North Carolina, USA. [4]Cantex Pharmaceuticals, Weston, Florida, USA.

Neuroblastoma prognosis is dependent on both the differentiation state and stromal content of the tumor. Neuroblastoma tumor stroma is thought to suppress neuroblast growth via release of soluble differentiating factors. Here, we identified critical growth-limiting components of the differentiating stroma secretome and designed a potential therapeutic strategy based on their central mechanism of action. We demonstrated that expression of heparan sulfate proteoglycans (HSPGs), including TβRIII, GPC1, GPC3, SDC3, and SDC4, is low in neuroblasts and high in the Schwannian stroma. Evaluation of neuroblastoma patient microarray data revealed an association between *TGFBR3*, *GPC1*, and *SDC3* expression and improved prognosis. Treatment of neuroblastoma cell lines with soluble HSPGs promoted neuroblast differentiation via FGFR1 and ERK phosphorylation, leading to upregulation of the transcription factor inhibitor of DNA binding 1 (ID1). HSPGs also enhanced FGF2-dependent differentiation, and the anticoagulant heparin had a similar effect, leading to decreased neuroblast proliferation. Dissection of individual sulfation sites identified 2-O, 3-O-desulfated heparin (ODSH) as a differentiating agent, and treatment of orthotopic xenograft models with ODSH suppressed tumor growth and metastasis without anticoagulation. These studies support heparan sulfate signaling intermediates as prognostic and therapeutic neuroblastoma biomarkers and demonstrate that tumor stroma biology can inform the design of targeted molecular therapeutics.

Introduction

Neuroblastoma, the most common cancer in infancy (1), arises from neural crest–derived sympathoadrenal precursor cells. Survival rates in late-stage disease are below 40% (2), due to disease recurrence and the persistence of residual tumor cells after cytotoxic therapy (3). Cellular differentiation and stromal content both strongly improve prognosis (4). The tumor stroma has been shown to release soluble factors that promote neuroblast differentiation and suppress tumor growth (5, 6), though their identity and the mechanism by which they act have not been elucidated. The clinical use of 13-*cis* retinoic acid to differentiate residual tumor cells, suppress their proliferation, and extend patient survival (7, 8) serves as proof of principle in the development of differentiation therapies for this disease (9–11).

We recently demonstrated that expression of the type III TGF-β receptor (TβRIII), a heparan sulfate proteoglycan (HSPG), promotes neuroblast differentiation to suppress proliferation, tumor growth, and metastasis (12). TβRIII acts via heparan sulfate binding to FGF2 and FGFR1 to enhance ERK MAPK signaling and expression of the transcription factor inhibitor of DNA binding 1 (ID1) (12). HSPGs, including the glypicans and syndecans, have demonstrated roles in neuronal development and nervous system FGF2 signaling (13–17) and are critical for cellular FGF responsiveness (18, 19). The roles of glypicans and syndecans in neuroblastoma pathogenesis have not been explored.

The anticoagulant heparin has potential utility as an antineoplastic agent via suppression of tumor angiogenesis and metastasis (20–23). Heparin promotes, and is often required for, FGF signaling (20, 24–27). Heparin is an intracellular variant of heparan sulfate that is composed of repeating glucosamine and glucuronic acid disaccharides sulfated at the 3-O, 6-O, and N- sites on glucosamine as well as at the 2-O site on glucuronic acid. These modifications are critical for heparin to bind antithrombin III and promote anticoagulation (25). Individual sulfation sites also mediate heparin effects on FGF signaling: specifically, the 2-O and N- sites are important for FGF2 binding, and the 6-O site is critical for FGFR binding (20, 25). The effects of heparin and its derivatives on FGF2 signaling and differentiation in neuroblasts have not been previously reported.

Here, we investigate the roles of HSPGs and FGF2 in neuroblastoma, identifying heparins as potential therapeutic agents.

Results

HSPG expression is localized to the stroma and decreased in neuroblastoma, with high expression associated with improved patient prognosis. Since TβRIII expression is decreased in neuroblastoma (12, 28–30), we determined mRNA expression of other HSPGs using our microarray meta-dataset (n = 213) (12). In comparison with benign neuroblastic tumors, expression of the HSPGs GPC1, GPC3,

Authorship note: Angela L. Gaviglio and Jasmine C. Nee contributed equally to this work.

Conflict of interest: Stephen G. Marcus is an employee and equity owner of Cantex Pharmaceuticals. Erik H. Knelson and Gerard C. Blobe disclose that they have submitted a US provisional patent application describing the development of heparin derivatives as therapeutic agents in neuroblastoma.

Note regarding evaluation of this manuscript: Manuscripts authored by scientists associated with Duke University, The University of North Carolina at Chapel Hill, Duke-NUS, and the Sanford-Burnham Medical Research Institute are handled not by members of the editorial board but rather by the science editors, who consult with selected external editors and reviewers.

Citation for this article: *J Clin Invest.* 2014;124(7):3016–3031. doi:10.1172/JCI74270.

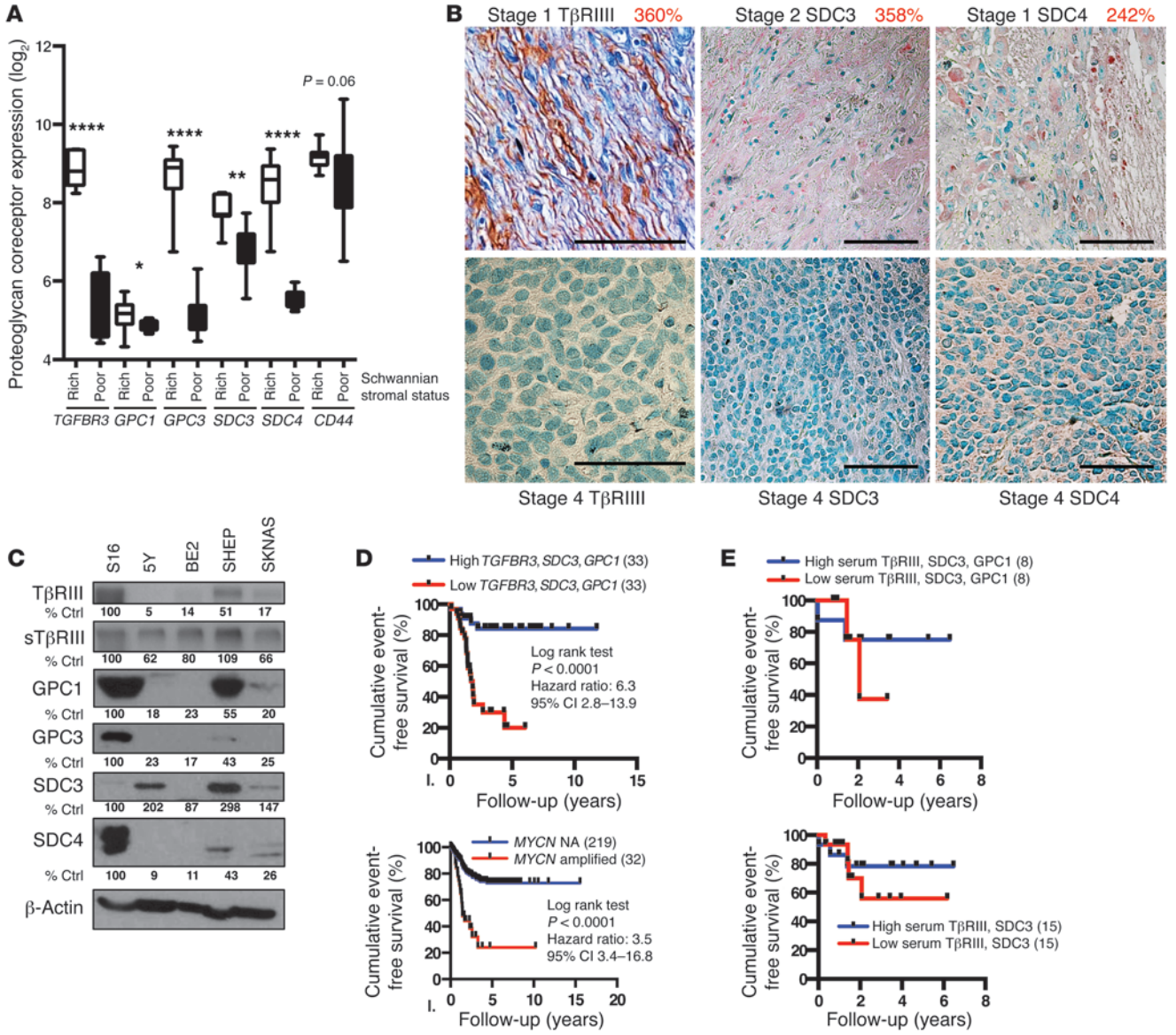

Figure 1

HSPG expression is localized to the stroma, and high expression is associated with improved patient prognosis. (**A**) Microarray dataset analysis (GSE7529) for HSPG expression in neuroblastic tumors based on stromal status (n = 8 stroma-rich, n = 11 stroma-poor). *P < 0.05; **P < 0.01; ****P < 0.0001 by Mann-Whitney U test. (**B**) IHC for TβRIII, SDC3, and SDC4 in the stroma of neuroblastoma tumor samples. HSPGs are labeled with red/pink stain, with methyl green nuclear counterstaining. Original magnification, ×60 (TβRIII); ×40 (SDC3 and SDC4); scale bars: 50 μM. Percentages shown indicate background-subtracted quantification of red channel densitometry in early-stage specimens relative to stage 4 specimens. (**C**) TGF-β binding and crosslinking with TβRIII pulldown for surface and sTβRIII in the indicated neuroblastoma cell lines, SHEP cells, and S16 Schwann cells. Western blots for GPC1, GPC3, SDC3, and SDC4 expression. Densitometry for HSPGs normalized to β-actin is shown as the percentage of control. (**D**) Analysis of event-free survival split by *TGFBR3*, then *SDC3*, then *GPC1* expression in the Obertheur dataset (denoted as l.) compared with stratification by *MYCN* status. NA, nonamplified. Low *HSPG* expression group: 12 of 33 *MYCN* amplified. High HSPG expression group: 1 of 33 *MYCN* amplified. (**E**) Serum ELISA for TβRIII, SDC3, and GPC1 using neuroblastoma patient samples (n = 60). Survival analysis split by TβRIII, then SDC3, then GPC1 soluble protein levels (blue: top 13%, red: bottom 13%), or by TβRIII, then SDC3 (blue: top 25%, red: bottom 25%). The differences between the survival curves were not statistically different by log-rank test.

SDC3, and SDC4 was decreased in neuroblastoma, with an additional significant decrease in TβRIII, SDC3, and SDC4 expression in late-stage compared with early-stage tumors (Supplemental Figure 1A and Supplemental Table 1; supplemental material available online with this article; doi:10.1172/JCI74270DS1).

In our previous work, TβRIII expression was readily detected in early-stage neuroblastoma patient specimens with high stromal content (12). To determine whether high HSPG expression was associated with high stromal content, we used a publicly available microarray dataset (GSE7529) that designates tumors as

stroma-rich or stroma-poor. We found that expression of TβRIII, GPC1, GPC3, SDC3, and SDC4 was significantly increased in stroma-rich tumors (Figure 1A). Subsequent microdissection by the authors isolated stromal and neuroblastic cells to generate a ranked list of proteins with higher stromal expression, which included TβRIII, GPC3, and SDC4 in the top 35 genes (ref. 31 and Supplemental Table 2). To investigate HSPG localization, we used immunohistochemistry (IHC) on patient samples (Figure 1B and Supplemental Figure 1B). TβRIII, GPC1, GPC3, SDC3, and SDC4 staining localized to the stroma in early-stage tumors, and these receptors were poorly expressed in late-stage specimens (Figure 1B and Supplemental Figure 1B). Immunofluorescence on patient samples demonstrated colocalization of HSPGs with stromal cells labeled by the Schwann cell marker S100 (refs. 6, 32, and Supplemental Figure 2). We then determined HSPG protein expression in neuroblastoma cell lines, along with SHEP and S16 cells used here as in vitro models of Schwannian stromal cells (5, 6, 33). TβRIII, GPC1, GPC3, SDC3, and SDC4 were more highly expressed in SHEP cells considered "S-type" or Schwannian (Figure 1C). TβRIII, GPC1, GPC3, and SDC4 were also highly expressed in the rat Schwann cell line S16 (Figure 1C; full, uncut gels are shown in the Supplemental Material). Using survival datasets (34, 35), we determined that high TβRIII, GPC1, and SDC3 expression conferred a significant survival advantage (ref. 12 and Supplemental Figure 1C). Furthermore, sequential stratification–based TβRIII, GPC1, and SDC3 expression identified a distinct patient subset with high receptor expression and excellent event-free survival (Figure 1D). As a prognostic biomarker, this 3-gene signature was comparable to *MYCN* oncogene amplification (Figure 1D). Soluble receptor levels in the sera of neuroblastoma patients demonstrated prognostic trends similar to those of the microarray data (Figure 1E and Supplemental Figure 1D).

Soluble HSPGs promote neuroblast differentiation. Since surface TβRIII expression promotes neuroblast differentiation via extracellular glycosaminoglycan modifications (12), we investigated whether soluble HSPGs (sHSPGs) could have similar effects. We used well-established models of neuroblast differentiation: neurite outgrowth in 5Y and BE2 cells (36, 37) and expression of neuron-specific proteins, including neurofilament 160 kDa in 5Y, BE2, and SK-N-AS cells (10, 38–40), neuron-specific enolase or tyrosine hydroxylase in 5Y cells (10, 41), and β3-tubulin in BE2 and SK-N-AS cells (42). Recombinant sTβRIII, sGPC1, sGPC3, sSDC3, and sSDC4 all enhanced neurite outgrowth in 5Y neuroblastoma cells (Figure 2, A and B, and Supplemental Figure 3, A–C). Likewise, sHSPGs promoted the expression of neuronal differentiation markers in multiple neuroblastoma cell lines (Figure 2, C–E, and Supplemental Figure 3, B–D). These effects were dose dependent (Figure 2E and Supplemental Figure 3C) and increased over time from 48 to 96 hours of treatment (Supplemental Figure 3B). Transient expression of sTβRIII, GPC1, or sGPC3 constructs also promoted neurite outgrowth and expression of differentiation markers in neuroblasts (Supplemental Figure 3E). Likewise, shRNA knockdown of GPC1 and SDC3 decreased the expression of neuronal differentiation markers (Supplemental Figure 3F). In our microarray meta-dataset, high HSPG expression was associated with high expression of the in vivo neuroblastoma differentiation markers SOX10 and ANXA2, as well as low expression of the primitive neuroectodermal marker ASCL1 (Figure 2F). These trends in expression of HSPGs and surrogate differentiation markers are consistent with TβRIII expression in patient samples, neuroblast differentiation, and response to differentiating agents (12, 40, 43, 44).

TβRIII and syndecans are modified with heparan and chondroitin sulfate, while glypicans only have heparan sulfate modifications (45). To determine whether the differentiating effects observed were generalizable to HSPGs, we treated cells with a nonspecific sHSPG mixture isolated from the extracellular matrix of sarcoma cells in culture. ELISA demonstrated no detectable sTβRIII and less than 1% sSDC3 in sHSPG (data not shown). sHSPG strongly promoted neuroblast differentiation (Figure 2, B–E), supporting the general ability of heparan sulfate to promote neuroblast differentiation.

Release of sHSPGs from Schwannian stromal cells in coculture promotes neuroblast differentiation. Since HSPGs are highly expressed in the stroma and promote neuroblast differentiation, we determined whether stroma-derived sHSPGs could promote neuroblast differentiation in a coculture model system. We used SHEP cells to model the Schwannian stroma (33), plating them in direct coculture suspended above 5Y cells, which were used to model neuroblasts (Supplemental Figure 4A). Coculture with SHEP, but not COS7, cells promoted neuronal differentiation in 5Y (Figure 3A). When TβRIII was overexpressed in SHEP, coculture further promoted differentiation in 5Y (Figure 3, A–C, and Supplemental Figure 4A). We observed a similar result using conditioned media from SHEP instead of direct coculture (Figure 3D and Supplemental Figure 4B). Enhanced differentiation was dependent on TβRIII glycosaminoglycan modifications (Supplemental Figure 4, A and C). When TβRIII was knocked down in SHEP, conditioned media from these cells failed to promote differentiation in 5Y (Figure 3D). SDC3 knockdown in SHEP also suppressed differentiation in both coculture and conditioned media experiments (Figure 3E and Supplemental Figure 4A), though to a lesser extent than TβRIII knockdown. To demonstrate that TβRIII shedding from SHEP was critical to coculture differentiation, we used a pharmacologic inhibitor of TβRIII shedding, TAPI2 (46). TAPI2 treatment suppressed TβRIII shedding from SHEP and subsequent differentiation of cocultured 5Y (Figure 3A and Supplemental Figure 4D).

sHSPGs enhance FGF2 signaling in neuroblasts to promote differentiation via ERK and ID1. Since TβRIII promotes neuroblast differentiation via glycosaminoglycan interaction with FGF2 and FGFR1 to enhance ERK/MAPK signaling and expression of the transcription factor ID1 (12), we investigated whether glypicans and syndecans promote differentiation via this pathway. Treatment with sTβRIII, sSDC3, sSDC4, or sHSPG enhanced basal as well as FGF2-induced neuronal differentiation, phosphorylation of ERK1/2, and expression of ID1 (Figure 4, A and B, and Supplemental Figure 5A). TβRIII, GPC1, GPC3, SDC3, and SDC4 expression each positively correlated with ID1 expression in our microarray meta-dataset (ref. 12, Figure 4C, and Supplemental Figure 5B), and multivariate regression analysis demonstrated that high expression of this group of receptors correlated with high ID1 expression in patient samples (Figure 4C).

To determine whether the differentiating effects of sHSPGs were via heparan sulfate modifications, we expressed a mutant sTβRIII construct with a single serine-to-alanine amino acid substitution to prevent heparan sulfate modification (S534A) (47). Expression of this construct failed to promote neuroblast differentiation (Figure 4D), indicating that heparan sulfate modifications are critical to the differentiating effects of sTβRIII.

To determine whether FGFR and MEK kinase activity were critical to the differentiating effects of sHSPGs, we cotreated neuro-

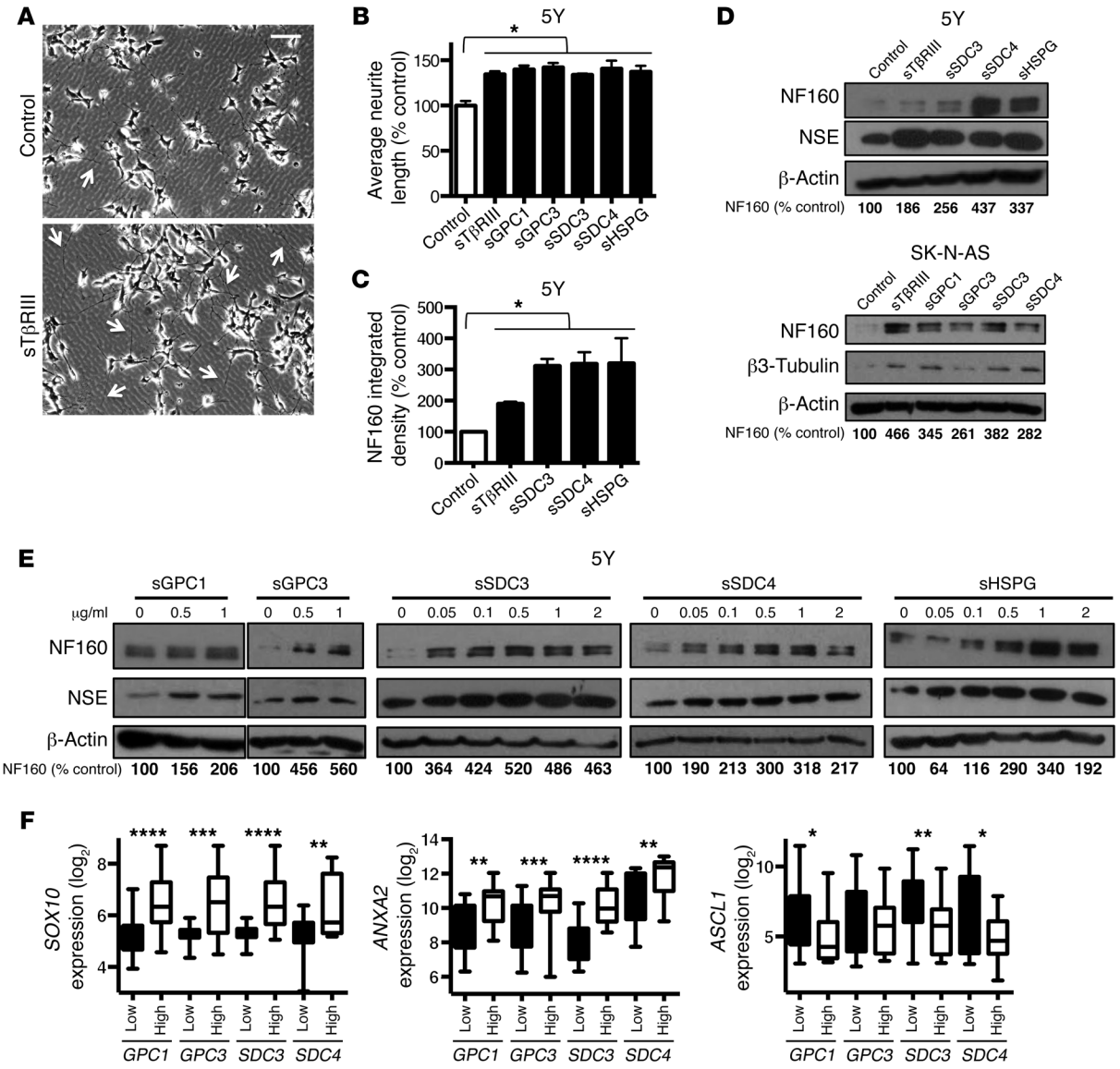

Figure 2

sHSPGs released from the stroma promote neuroblast differentiation. (**A**) Phase-contrast images of 5Y cells after 96 hours of treatment with sTβRIII. Arrows identify abnormally long neurites (>2 times the mean neurite length). Original magnification, ×10; scale bar: 100 μm. (**B**) Quantification of neurite length using NeuronJ after a 72-hour treatment with sTβRIII (10 ng/ml), sSDC3, sSDC4, or sHSPG (1 μg/ml). Data are presented as the mean of 3 fields ± SEM. $P < 0.01$ by ANOVA; $^*P < 0.05$ by Bonferroni-corrected *t* test. (**C**) Quantification of NF160 densitometry normalized to β-actin from 3 independent Western blots after 72 hours of treatment with 10 ng/ml sTβRIII or 1 μg/ml sSDC3, sSDC4, or sHSPG, normalized to β-actin and presented as the mean ± SEM. $^*P < 0.05$ by 1-sample Student's *t* test. (**D**) Western blots for differentiation markers after 72 hours of treatment with 10 ng/ml sTβRIII or 1 μg/ml sGPC1, sGPC3, sSDC3, sSDC4, or sHSPG. Densitometry for NF160 normalized to β-actin is shown as the percentage of control. (**E**) Western blots for differentiation markers after 72 hours of treatment with sHSPGs (1 μg/ml). Densitometry for NF160 normalized to β-actin is shown as the percentage of control. (**F**) Microarray meta-dataset expression of *SOX10*, *ANXA2*, and *ASCL1* in low (bottom 10%) and high (top 10%) HSPG–expressing tumors (median and interquartile range). $^{****}P < 0.0001$; $^{***}P < 0.001$; $^{**}P < 0.01$; $^*P < 0.05$ by Mann-Whitney *U* test. *SDC4* data are from the 3 U133 Plus datasets only.

blastoma cells with inhibitors of FGFR kinase activity (SU5402, PD173074) or downstream MEK kinase activity (U0126, CI1040). All treatments prevented the differentiating effects of sTβRIII and sSDC3 (Figure 4E). We found that expression of dominant negative FGFR1 also suppressed HSPG-induced differentiation (Figure 4E).

To determine whether additional downstream signaling pathways were activated in response to treatment with FGF2, we performed Western blotting for signaling mediators downstream of FGFR1 and TβRIII in neurons (12, 48). We used BMP2 as a ligand control. Consistent with our previous results, FGF2 and sTβRIII synergistically promoted neuroblast differentiation in conjunction with increased phosphorylation of FGFR1 and ERK (Supplemental Figure 7B). As expected, we also observed increases in phosphorylation of AKT and STAT3 following FGF2 treatment, but

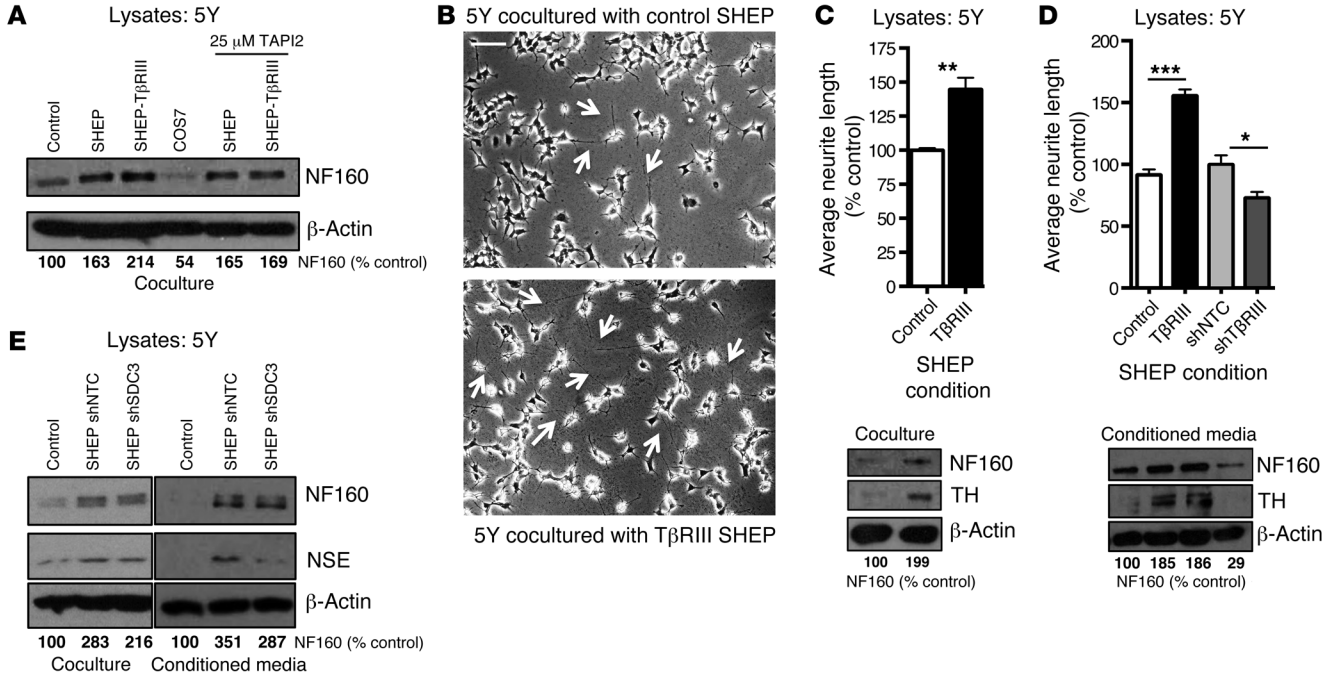

Figure 3

Release of sHSPGs from Schwannian stromal cells in coculture promotes neuroblast differentiation. (**A**) Western blot for differentiation markers in 5Y after 72 hours of coculture with SHEP, COS7, or SHEP expressing a control GFP or a TβRIII-GFP construct. TAPI2 treatment of SHEP was added to the upper Transwell. Densitometry for NF160 normalized to β-actin is shown as the percentage of control. (**B**) Phase-contrast images of 5Y neurites after 72 hours of coculture. Arrows identify abnormally long neurites (>2 times the mean neurite length). Original magnification, ×10; scale bar: 100 μM. (**C**) Quantification of neurite length from 3 fields using NeuronJ software. Data are presented as the mean of 3 fields ± SEM. $^*P < 0.05$; $^{**}P < 0.01$; $^{***}P < 0.001$ by 2-tailed Student's *t* test. Western blot for differentiation markers in 5Y after 72 hours of coculture with SHEP expressing GFP or TβRIII-GFP. Densitometry for NF160 normalized to β-actin is shown as the percentage of control. (**D**) Western blot for differentiation markers in 5Y after 72 hours of treatment with conditioned media from SHEP expressing a nontargeted control shRNA construct (shNTC) or shRNA targeted to TβRIII (shTβRIII). Densitometry for NF160 normalized to β-actin is shown as the percentage of control. (**E**) Western blot for differentiation markers in 5Y after 72 hours of coculture or treatment with conditioned media from SHEP expressing a nontargeted control shRNA construct (shNTC) or shRNA targeted to SDC3 (shSDC3). Densitometry for NF160 normalized to β-actin is shown as the percentage of control.

sTβRIII treatment neither activated these pathways nor provided synergy with FGF2 (Supplemental Figure 7B). Both BMP2 and FGF2 treatment mildly increased p38 and SMAD1 phosphorylation, but again failed to synergize with sTβRIII (Supplemental Figure 7B). Neither BMP2 nor FGF2 treatment substantially altered SMAD3 phosphorylation (Supplemental Figure 7B). In summary, the only signaling effects that tracked with differentiation markers were phosphorylation of FGFR1 and ERK, which supports our pharmacologic inhibitor, knockdown, and dominant negative receptor studies demonstrating that this pathway is responsible for heparan sulfate–induced neuroblast differentiation.

FGF2 is a critical component of the differentiating stroma secretome and a potential serum prognostic marker. We next determined the importance of FGF2 ligand expression in stroma-induced differentiation. The neuroblastoma patient specimens and microarray data showed that FGF2 localized to the stroma (Figure 5, A–C, and Supplemental Figure 2). FGF2 was also highly expressed in the Schwannian cell lines SHEP and S16 (Figure 5C). We analyzed the expression of a panel of HSPG-binding growth factors in tumors with high and low stromal content and found that FGF2 was most differentially expressed (Supplemental Figure 6A). IGF1, which has been shown to promote neuroblast differentiation (49), and heparin-binding EGF (HBEGF) were also significantly upregulated in stroma-rich tumors (Supplemental Figure 6A). Within the FGF signaling family, FGF1 and FGF7, both of which bind heparan sulfate, were also more highly expressed in stroma-rich tumors (Supplemental Figure 6B). Knockdown of FGF2 abrogated the differentiating effects of SHEP-conditioned media (Figure 5D and Supplemental Figure 4E), suggesting that FGF2 is critical to the differentiating effects of the stroma. We found that serum FGF2 levels were elevated in a subset of neuroblastoma patients, compared with those in pediatric controls, and that high serum FGF2 levels were associated with improved prognosis (Figure 5, E and F). These data support our hypothesis that the neuroblastoma stroma releases FGF2, as well as sHSPGs, to promote neuroblast differentiation via FGFR1, ERK, and ID1 (Figure 5G). Stromal release of FGF2 may alter serum levels, identifying a potential prognostic serum marker for neuroblastoma patients.

Heparin promotes neuroblast differentiation via FGFR1, ERK, and ID1. As HSPGs were able to promote neuroblast differentiation, we investigated whether heparin treatment could have similar effects. Indeed, heparin promoted neurite outgrowth and expression of neuronal differentiation markers in a dose-dependent fashion in multiple neuroblastoma cell lines, with potency and kinetics similar to those of sHSPGs (Figure 6, A and B). Heparin treatment enhanced FGF2-induced differentiation, ERK phosphorylation,

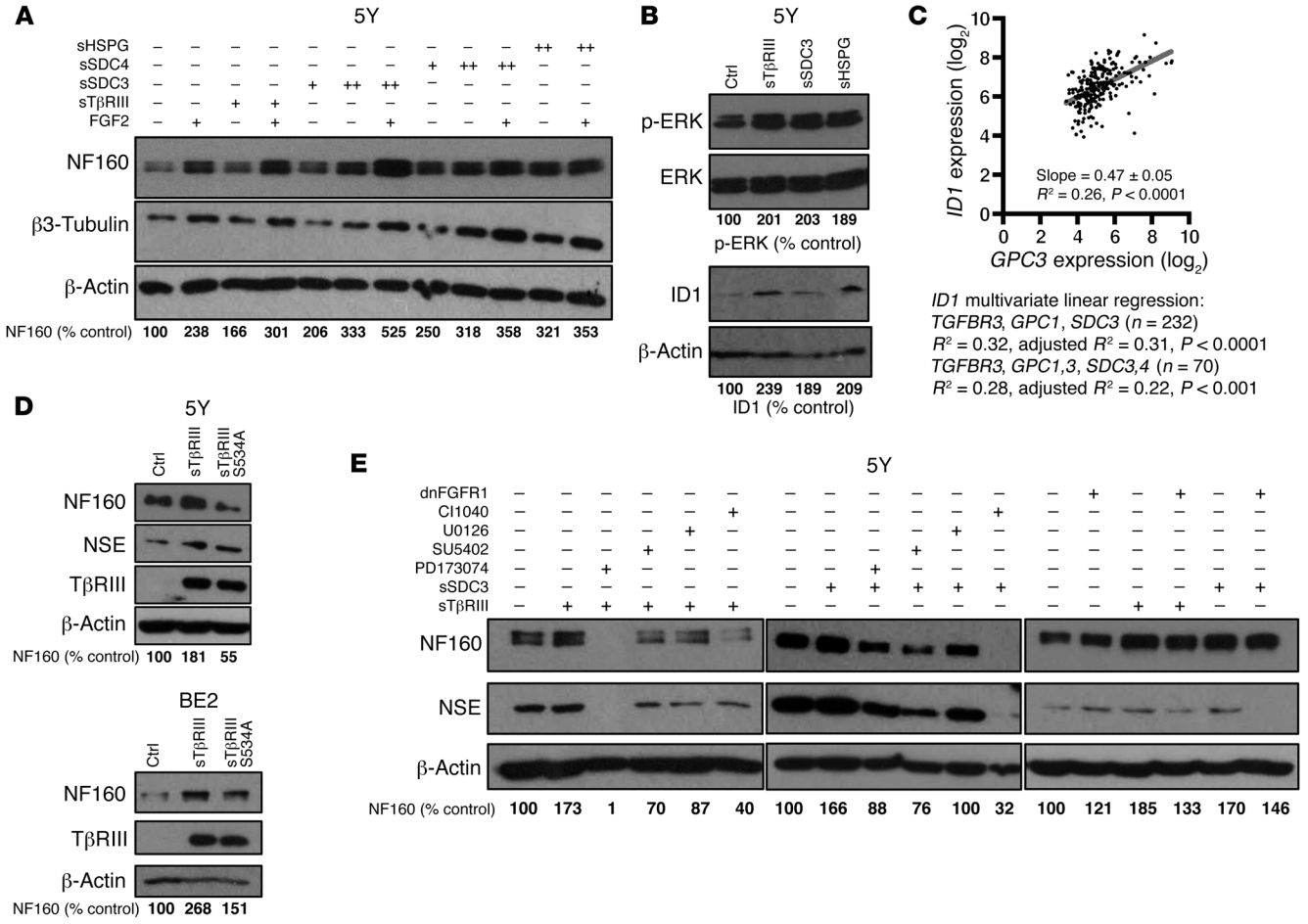

Figure 4

sHSPGs enhance FGF2 signaling in neuroblastoma cells to promote differentiation via ERK and ID1. (**A**) Western blots for differentiation markers in 5Y treated for 96 hours with 1 ng/ml FGF2, sTβRIII (10 ng/ml), sSDC3, sSDC4, or sHSPG (+100 ng/ml or ++1 μg/ml). Densitometry for NF160 normalized to β-actin is shown as the percentage of control. (**B**) Western blots for phosphorylated and total ERK as well as ID1 in 5Y treated for 96 hours with sTβRIII (10 ng/ml), sSDC3, or sHSPG (1 μg/ml). Densitometry for p-ERK and ID1 normalized to β-actin is shown as the percentage of control. (**C**) Linear regression and multivariate regression analyses using the microarray meta-dataset. (**D**) Western blots for differentiation markers and TβRIII in cells transfected for 96 hours with wild-type sTβRIII or sTβRIII with a single amino acid substitution to prevent heparan sulfate modification (TβRIII S534A). Densitometry for NF160 normalized to β-actin is shown as the percentage of control. (**E**) Western blots for differentiation markers in 5Y treated for 96 hours with sTβRIII (10 ng/ml), sSDC3 (1 μg/ml), PD173074, UO126, CI1040 (1 μM), or SU5402 (10 μM). Transient transfection with dominant negative FGFR1 (dnFGFR1) or IRES-GFP control. GFP fluorescence was used to confirm construct expression. Densitometry for NF160 normalized to β-actin is shown as the percentage of control.

and expression of ID1 over the time course of differentiation (Figure 6B and Supplemental Figure 7C). Treatment with FGFR or MEK kinase inhibitors or expression of dominant negative FGFR1 suppressed these differentiating effects (Figure 6C). Ligand binding may be necessary for the differentiating effects of heparin, since coincubation with an FGF2-inhibitory antibody (Supplemental Figure 7G) prevented differentiation. Interestingly, we found that heparin promoted differentiation of SK-N-AS cells, which are insensitive to retinoic acid (refs. 50, 51, and Figure 6, B and C). The differentiating effects of heparin and retinoic acid were additive in the retinoic acid–sensitive cell lines 5Y and BE2 (Supplemental Figure 7H). Heparin was more potent than retinoic acid over a long time course and increased expression of the neuronal differentiation marker neuron-specific enolase, which retinoic acid did not alter (Supplemental Figure 7H).

sHSPGs and heparin suppress neuroblast proliferation and orthotopic xenograft growth. Since neuroblast differentiation suppresses proliferation (10, 36–42), we determined whether treatment with sHSPGs and heparin could suppress neuroblast proliferation. We found that sHSPG and heparin treatment increased expression of the cell-cycle repressor protein p21 over the time course of differentiation and enhanced FGF2-induced p21 expression (Figure 7A and Supplemental Figure 8A). Microarray data demonstrated that high GPC1, GPC3, SDC3, and SDC4 expression was associated with enhanced regulation of cell-cycle progression, including increased p21 expression (Figure 7B, Supplemental Figure 8B, and ref. 12). To further assess the early effects of sHSPG and heparin treatment on proliferation, we performed thymidine incorporation after 24 hours of treatment. sTβRIII, sHSPG, and heparin suppressed proliferation by 30% to 60% (Figure 7C). The effects of

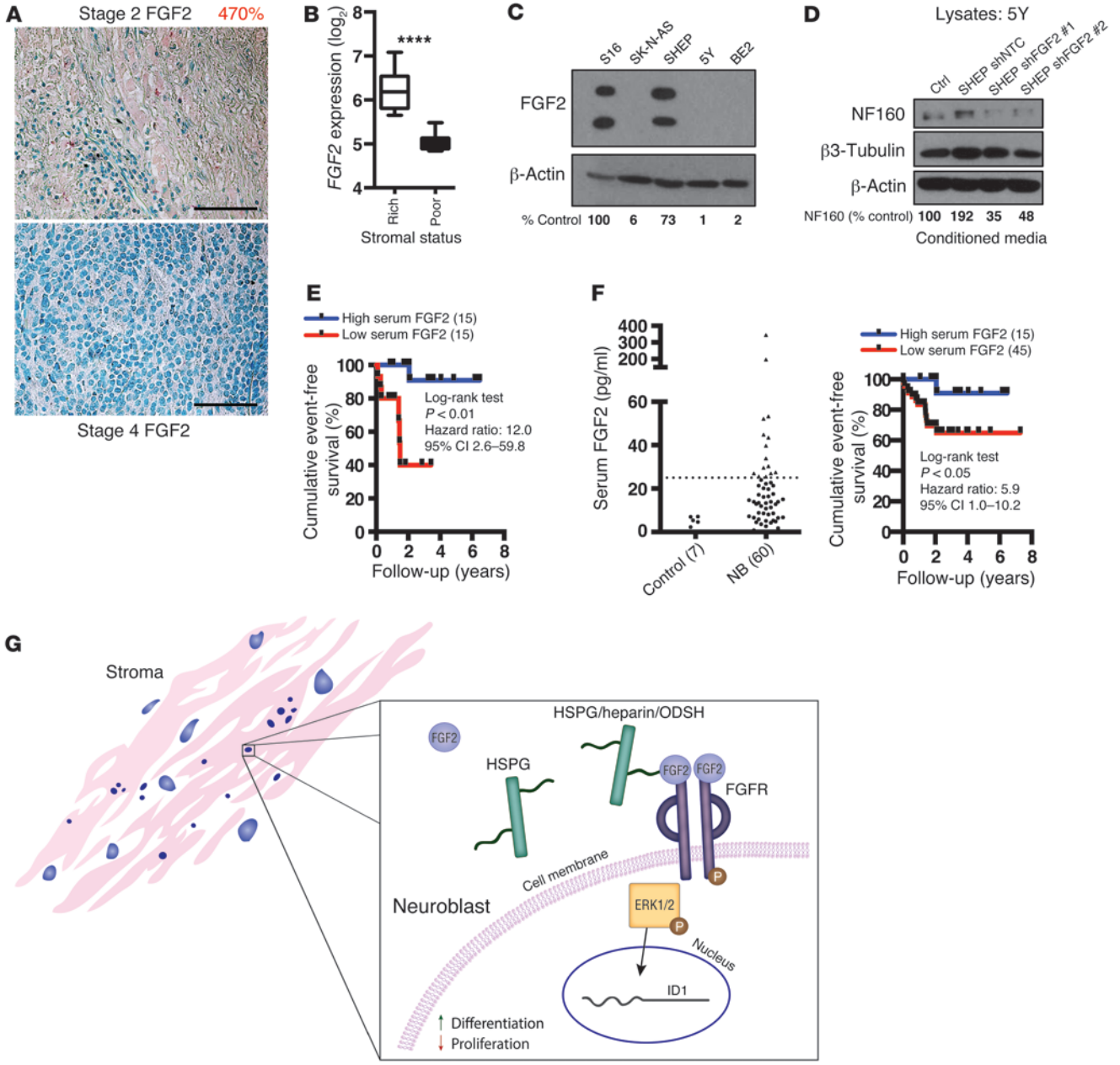

Figure 5

FGF2 is a critical component of the differentiating stroma secretome and a potential serum prognostic marker. (**A**) FGF2 IHC in the stroma of an early-stage neuroblastoma tumor sample. FGF2 is labeled with red/pink stain, with methyl green nuclear counterstaining. Original magnification, ×40; scale bars: 50 μM. Percentage shown indicates background-subtracted quantification of red channel densitometry relative to the stage 4 specimen. (**B**) Microarray dataset analysis (GSE7529) for *FGF2* expression in neuroblastic tumors based on stromal status (n = 8 stroma-rich, n = 11 stroma-poor). ****$P < 0.0001$ by Mann-Whitney U test. (**C**) Western blot for FGF2 expression in the indicated neuroblastoma cell lines, SHEP cells, and S16 Schwann cells. Densitometry for FGF2 normalized to β-actin is shown as the percentage of control. (**D**) Western blot for differentiation markers in 5Y after 72 hours of treatment with conditioned media from SHEP expressing a nontargeted control shRNA construct (shNTC) or shRNA targeted to FGF2 (shFGF2 #1 and #2). Densitometry for NF160 normalized to β-actin is shown as the percentage of control. (**E**) Serum ELISA for FGF2 using neuroblastoma patient samples (n = 60). Survival analysis split by quartile (blue: top 25%, red: bottom 25%). (**F**) Serum ELISA for FGF2 using neuroblastoma patient samples (NB; n = 60) and control pediatric remnant samples (n = 7). Survival analysis split by raw serum value (pg/ml; blue: >25 pg/ml, red: <25 pg/ml). (**G**) Schematic of the differentiating stroma secretome and resultant signaling changes in neuroblasts.

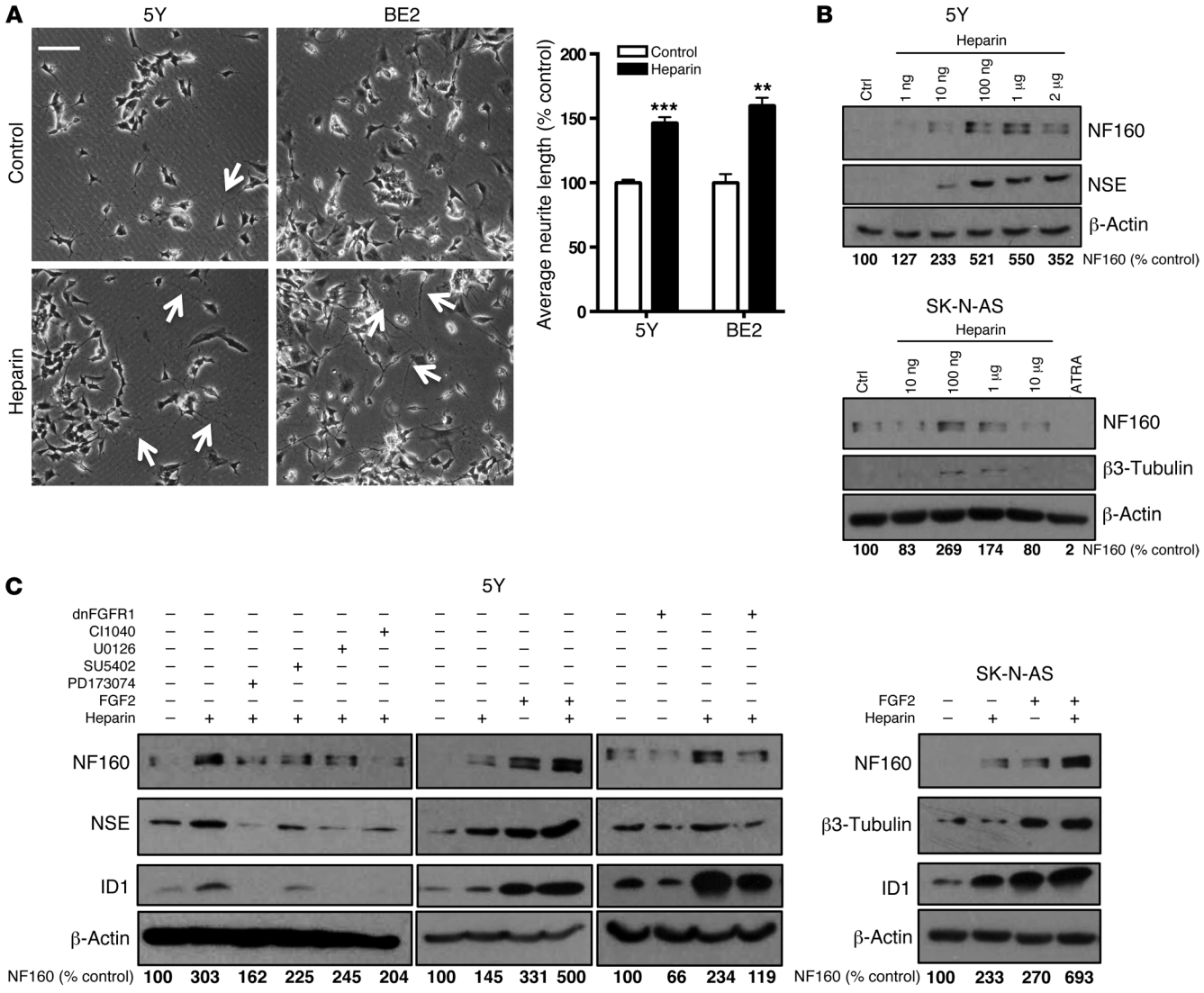

Figure 6

Heparin promotes neuroblast differentiation via FGFR1, ERK, and ID1. (**A**) Phase-contrast images of 5Y and BE2 cells after 72 hours of heparin treatment (1 μg/ml). Arrows identify abnormally long neurites (>2× the mean neurite length). Original magnification, ×10; scale bar: 100 μm. Quantification of neurite length using NeuronJ software. Data are presented as the mean of 3 fields ± SEM. $^{**}P < 0.01$, $^{***}P < 0.001$ versus control, by 2-tailed Student's *t* test. (**B**) Western blots for differentiation markers in 5Y and SK-N-AS treated for 72 hours with a dose course of heparin or ATRA (10 μM). Densitometry for NF160 normalized to β-actin is shown as the percentage of control. (**C**) Western blots for differentiation markers and ID1 in 5Y and SK-N-AS treated for 72 hours with heparin (1 μg/ml), FGF2 (1 ng/ml), PD173074, UO126, CI1040, or SU5402 (1 μM). Transient transfection with dominant negative FGFR1 or IRES-GFP control. GFP fluorescence was used to confirm construct expression. Densitometry for NF160 normalized to β-actin is shown as the percentage of control.

heparin were dose dependent, more potent than soluble receptor treatment, and reproducible across multiple neuroblastoma cell lines (Figure 7, C–E). We found that heparin had no effect on proliferation in control cell lines, including epithelial, embryonal, and cancer cells (Figure 7E). Heparin also suppressed tumor growth and extended survival in vivo in an orthotopic model of neuroblastoma (Figure 7F). These effects were limited by enhanced sensitivity to anticoagulation in tumor-bearing mice and subsequent dose reduction (see Discussion).

Heparan sulfation is associated with improved patient prognosis and critical to its differentiating and antiproliferative effects. To determine whether heparan sulfation influences neuroblastoma prognosis, we analyzed sulfyltransferase expression in patient microarray data. High expression of the 2-O sulfyltransferase HS2ST1 and the 6-O sulfyltransferases HS6ST2 and HS6ST3, as well as the N-deacetylase/N-sulfyltransferase NDST2, was associated with improved patient survival in multiple datasets (Figure 8A and Supplemental Figure 9A). Conversely, high expression of the sulfatases SULF1 and SULF2 was associated with poor survival (Supplemental Figure 9B). These data support the importance of heparan sulfation in neuroblastoma pathogenesis. High expression of heparan sulfate extension enzymes, which play no role in

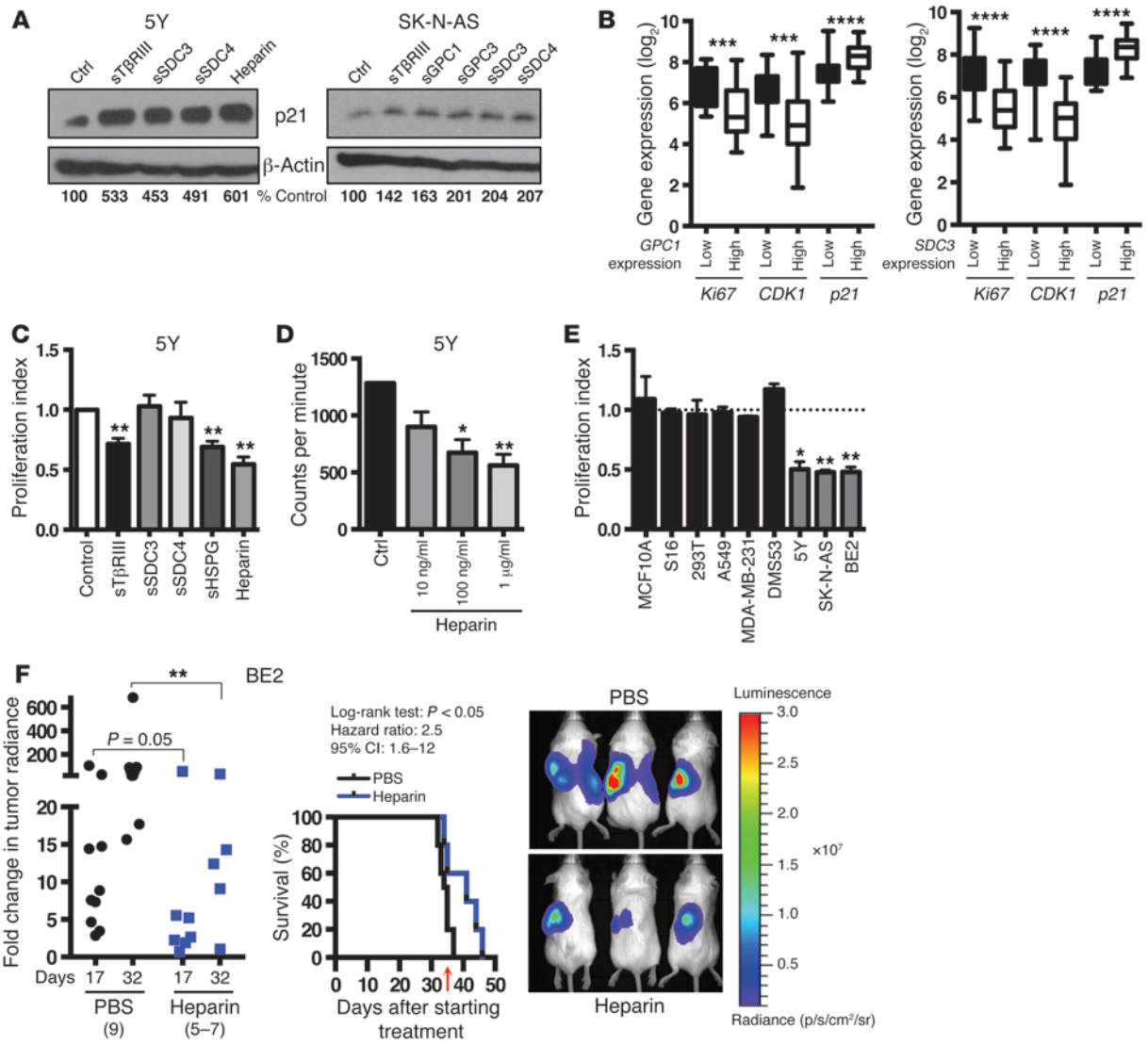

Figure 7

sHSPGs and heparin suppress neuroblast proliferation. (**A**) Western blot for p21 in 5Y treated for 96 hours and SK-N-AS treated for 72 hours with sTβRIII (10 ng/ml), sGPC1, sGPC3, sSDC3, sSDC4, or heparin (1 μg/ml). Densitometry for p21 normalized to β-actin is shown as the percentage of control. (**B**) Microarray meta-dataset expression of cell-cycle genes in low *GPC1*– or *SDC3*–expressing tumors (bottom 10%; shaded) versus high *GPC1*– or *SDC3*–expressing tumors (top 10%; unshaded). Data are presented as the median and interquartile ranges. ***$P < 0.001$; ****$P < 0.0001$ by Mann-Whitney *U* test. (**C**) Thymidine incorporation after a 24-hour treatment with sTβRIII (10 ng/ml), sSDC3, sSDC4, sHSPG, or heparin (1 μg/ml). Data are normalized to the control untreated cells (proliferation index 1.0) and presented as the mean ± SEM of 4 replicates. **$P < 0.01$ by 1-sample Student's *t* test. (**D**) Average scintillation counts per minute with increasing doses of heparin (24-hour treatment). Data are presented as the mean ± SEM of 3 replicates. One-way ANOVA, $P < 0.01$; *$P < 0.05$ and **$P < 0.01$ by 2-tailed Student's *t* test. (**E**) Proliferation index for neuroblastoma and control cell lines after a 24-hour treatment with 1 μg/ml heparin. Data are normalized to the control untreated cells and presented as the mean ± SEM of 3 replicates. *$P < 0.05$; **$P < 0.01$ by 1-sample Student's *t* test. (**F**) BE2 orthotopic xenograft. Tumor radiance was measured after 32 days of growth using luciferase imaging (photons/s/cm²/steradian). Radiance was measured again after 17 and 32 days of treatment with PBS or 0.25 mg/mouse/day of heparin, and fold change in tumor radiance was calculated. **$P < 0.01$ versus PBS control by Mann-Whitney *U* test. Survival until humane endpoints as a percentage of each condition. Treatment was stopped after 35 days (red arrow). Bioluminescence images after 17 days of treatment.

sulfation but contribute to saccharide length, did not alter prognosis (Supplemental Figure 9C).

Since 2-O- and N-sulfation promote FGF2 binding and 6-O-sulfation mediates FGFR binding (20, 25), we used selectively desulfated heparins (2DES, 6DES, and NDES) to investigate which modifications were critical to the differentiating and antiproliferative effects of heparin. Selective 6-O- and N-sulfate removal abrogated the differentiating and antiproliferative effects of heparin (Figure 8B and Supplemental Figure 8C). Selectively 2-O-desulfated heparin (2DES) retained the ability to differentiate neuroblasts but had diminished antiproliferative effects (Figure 8B and Supplemental Figure 8C). Taken together, these results demon-

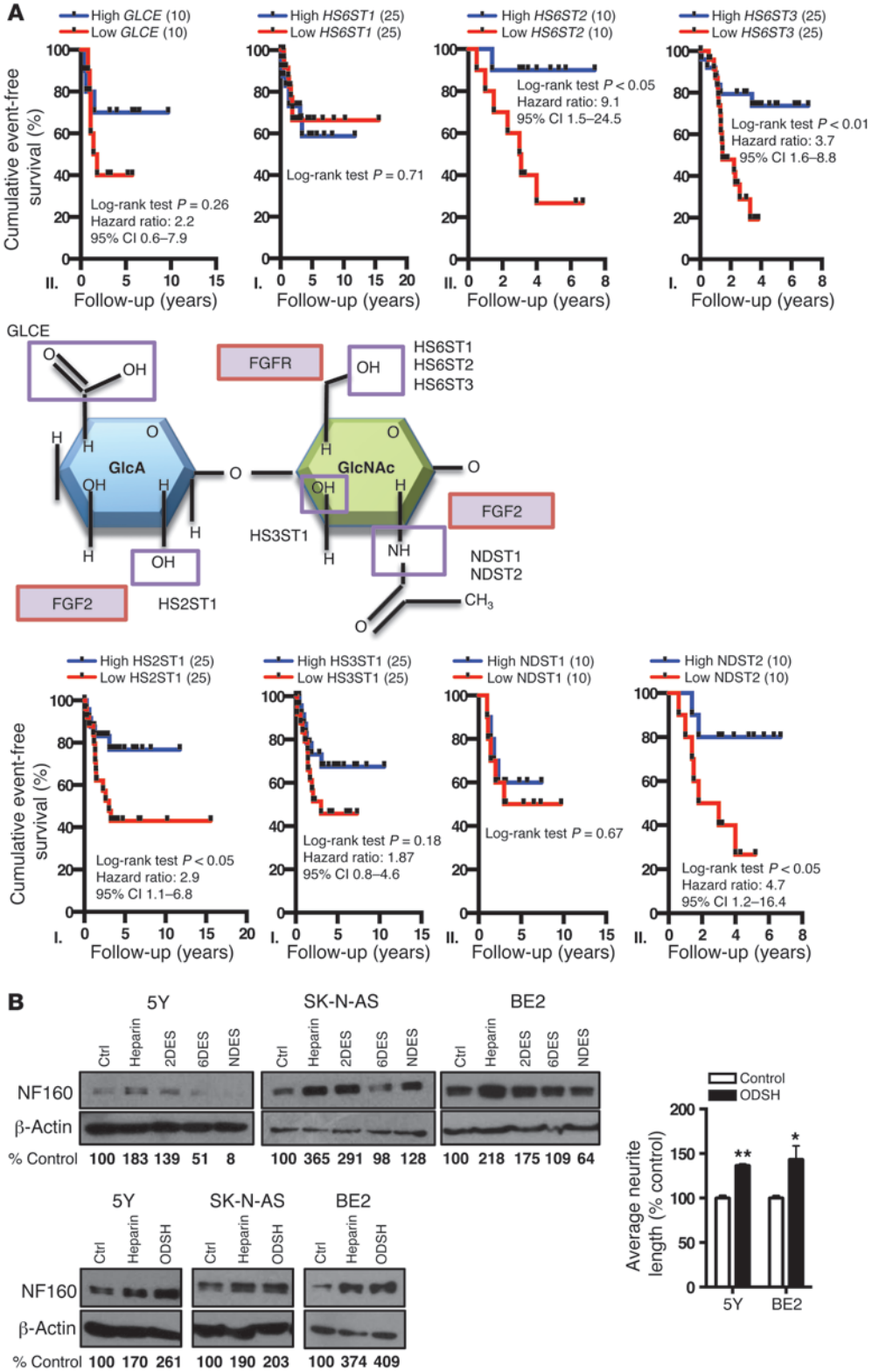

Figure 8

Dissection of heparin sulfation sites identifies ODSH as a differentiating agent. (**A**) Analysis of event-free survival split by epimerase and sulfyltransferase expression in the Obertheur dataset (denoted as I. blue = top 10%; red = bottom 10%) and the neuroblastoma prognosis dataset (denoted as II. blue = top 20%; red = bottom 20%) using oncogenomics software. Schematic of heparin sulfation dependent on the N-, 2-, 3-, and 6-sulfyltransferases as well as on the epimerase GLCE. Red-framed boxes indicate sulfation events that allow FGF2 and FGFR binding. (**B**) Western blots for NF160 in neuroblastoma cell lines treated with heparin and desulfated heparins (1 μg/ml). Quantification of neurite length using NeuronJ software after a 72-hour treatment with ODSH (1 μg/ml). Data are presented as the mean of 3 fields ± SEM. $^{*}P < 0.05$; $^{**}P < 0.01$ versus control by 2-tailed Student's *t* test. Densitometry for NF160 normalized to β-actin is shown as the percentage of control.

strate that 6-O- and N-sulfation are critical to the differentiating and antiproliferative effects of heparin, whereas 2-O-sulfation may be dispensable for differentiating effects, perhaps due to redundancy with N-sulfation in FGF2 binding.

2-O, 3-O-desulfated heparin promotes differentiation to suppress neuroblastoma orthotopic xenograft growth and metastasis while avoiding anticoagulation. The anticoagulant activity of heparin represents a barrier to clinical use in neuroblastoma, as demonstrated by dosing chal-

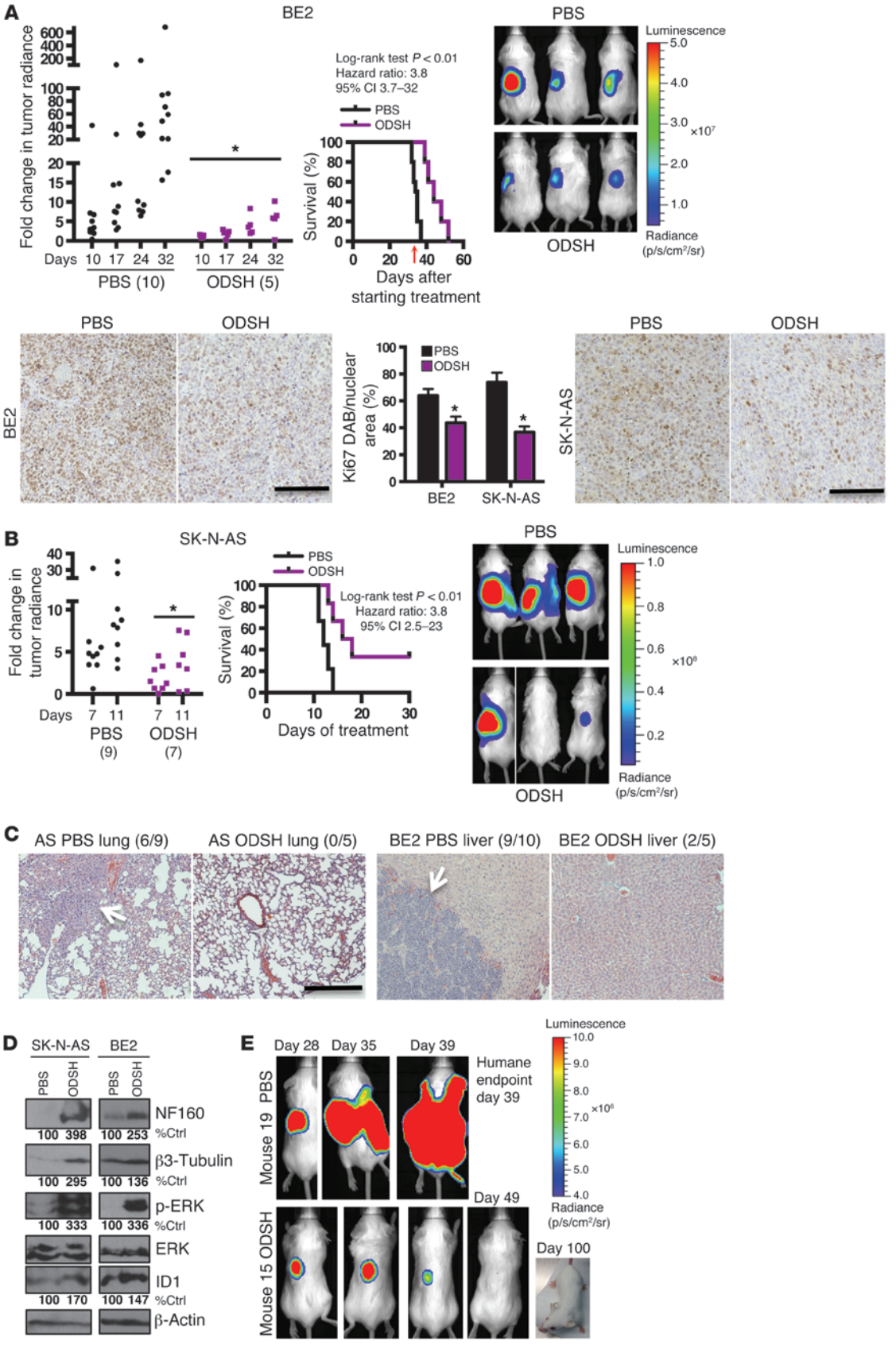
A
BE2
Fold change in tumor radiance
Days 10 17 24 32 10 17 24 32
PBS (10)
ODSH (5)
Log-rank test P < 0.01
Hazard ratio: 3.8
95% CI 3.7–32
PBS
ODSH
Survival (%)
Days after starting treatment
PBS
ODSH
Luminescence
Radiance (p/s/cm²/sr)
BE2
SK-N-AS
Ki67 DAB/nuclear area (%)
B
SK-N-AS
Fold change in tumor radiance
Days 7 11 7 11
PBS (9)
ODSH (7)
Log-rank test P < 0.01
Hazard ratio: 3.8
95% CI 2.5–23
Days of treatment
C
AS PBS lung (6/9)
AS ODSH lung (0/5)
BE2 PBS liver (9/10)
BE2 ODSH liver (2/5)
D
SK-N-AS
BE2
NF160
β3-Tubulin
p-ERK
ERK
ID1
β-Actin
%Ctrl
E
Day 28
Day 35
Day 39
Day 49
Day 100
Humane endpoint day 39
Mouse 19 PBS
Mouse 15 ODSH

Figure 9
ODSH suppresses neuroblastoma orthotopic xenograft growth and metastasis. (**A**) BE2 orthotopic xenograft. Tumor radiance was measured after 32 days of growth using luciferase imaging (photons/s/cm^2/steradian), and the measurement was used to calculate the fold change in tumor radiance after 10, 17, 24, and 32 days of treatment with PBS or 1 mg/mouse/day of ODSH. Mann-Whitney *U* test, **P* < 0.05 versus control at all time points. Luminescence images on day 24 of treatment. Survival until humane endpoints as a percentage of each condition. Treatment was stopped after 35 days (red arrow). Ki67 staining of xenograft sections. Original magnification, ×20; scale bar: 50 μM. Quantification of stain intensity using ImmunoRatio software. Data are presented as the mean of 3 sections ± SEM. **P* < 0.05 versus control by 2-tailed Student's *t* test. (**B**) SK-N-AS orthotopic xenograft. Tumor radiance was measured after 28 days of growth using luciferase imaging (photons/s/cm^2/steradian), and the measurement was used to calculate the fold change after 7 and 11 days of treatment with PBS or 1 mg/mouse/day of ODSH. Luminescence images on day 7 of treatment. Survival until humane endpoints as a percentage of each condition. (**C**) H&E-stained organs from xenografted mice treated with PBS control or ODSH. Parentheses indicate the number of mice with AS or BE2 cell metastasis to the indicated organ. Arrows point to metastases. Original magnification, ×10; scale bar: 200 μM. (**D**) Western blots for differentiation and signaling markers in lysates from SK-N-AS and BE2 xenografts. Densitometry normalized to β-actin is shown as the percentage of control. (**E**) Images of tumor radiance in a pair of mice with a similar original tumor size in the SK-N-AS experiment. Injections were stopped after 32 days of treatment (day 60).

lenges in our xenograft model. Since HSPGs, 2DES, and heparin all promoted neuroblast differentiation, we determined whether heparin derivatives that lack anticoagulant activity retain differentiating and tumor-suppressive potency. Using our model systems, we tested 2-O, 3-O-desulfated heparin (ODSH), which has antimetastatic activity in models of pancreatic cancer and melanoma and is clinically well tolerated, with less than 5% of the anticoagulation seen with fully modified heparin (52). In neuroblastoma cell lines, ODSH promoted neuronal differentiation via FGFR1 and ERK phosphorylation to upregulate ID1 expression and mildly suppressed proliferation over a 24-hour period (Figure 8B, Supplemental Figure 7, A, B, D, F, and Supplemental Figure 8C). ODSH treatment rescued decreases in differentiation markers following TβRIII and GPC1 knockdown (Supplemental Figure 7E), suggesting that it could reverse the effects of decreased HSPG expression in tumors. We found that the differentiating effects of ODSH depended on FGFR1 and FGF2, as demonstrated by shRNA-mediated silencing of ligand and receptor expression (Supplemental Figure 7F). In 2 orthotopic xenograft models with a 4-week treatment delay to allow for tumor engraftment, 1 mg/mouse/day of ODSH suppressed tumor growth and metastasis and extended survival without anticoagulant side effects (Figure 9, A–C, and Supplemental Figure 9, D–G). Western blot analysis of tumor lysates demonstrated enhanced expression of differentiation markers, phosphorylation of ERK, and upregulation of ID1 in tumors from mice treated with ODSH (Figure 9D). In our BE2 model, ODSH treatment was more potent than dose-reduced heparin or 20 μg/kg/day fenretinide, which is used clinically (53) and can suppress BE2 orthotopic xenograft growth (ref. 54 and Supplemental Figure 9D). In our SK-N-AS model, 2 ODSH-treated mice demonstrated a complete response (Figure 9E), supporting the potential utility of modified heparins as therapeutic agents for neuroblastoma patients.

Discussion

Here, we used tumor stroma biology to identify heparin as a differentiating agent in neuroblastoma. In addition, we established that desulfated heparin derivatives, including ODSH, may prove clinically useful as differentiating agents, while avoiding unwanted anticoagulation. We describe in vitro screening techniques to identify differentiating agents with FGF signaling activity that can suppress tumor growth and metastasis in animal models. We used these tools to uncover critical components of the differentiating stroma secretome, including HSPGs and their ligand FGF2. High tumor expression levels and serum concentrations of these proteins are associated with improved prognosis and could be used as prognostic and therapeutic biomarkers in neuroblastoma patients.

While neuroblastoma cell lines have provided useful model systems to study neuroblast differentiation in vitro, leading to the identification of retinoic acid as a clinical therapeutic (55), no additional therapies have emerged (10). Moreover, while pathways regulating neuroendocrine differentiation in development are well described (56), the precise roles of these pathways in neuroblastoma pathogenesis remain unclear. The tumor stroma, composed primarily of Schwann cells, can suppress tumor growth by reactivating developmental differentiation pathways. Previous experiments using Schwann cell coculture or conditioned media (5, 57–60), as well as studies of neuroblastoma xenografts implanted in the mouse nerve sheath (6), demonstrate that Schwann cells release soluble differentiating and antiangiogenic factors to suppress neuroblast proliferation and tumor growth. Here, we identify HSPGs, their ligand FGF2, and FGFR/ERK signaling as critical to stroma-induced neuroblast differentiation (Figures 1–5). SDC3 (N- or neuronal syndecan) was initially cloned from rat Schwann cells and has been implicated in nervous system development and neuronal FGF2 signaling (13–15). While both GPC1 and SDC3 promote neurite outgrowth (16, 17), they have not been implicated in neuroblastoma pathogenesis. Here, we demonstrated that expression of GPC1 and SDC3 was high in stromal cells and low in neuroblasts and that high expression of these HSPGs was associated with improved patient prognosis (Figure 1). These studies suggest that HSPGs and their ligand FGF2 may be important in neuronal development.

The central mechanism we have identified for the differentiating effects of heparin and HSPGs involves binding FGF2 and FGFR1, leading to increased ERK phosphorylation and upregulation of ID1 (Figures 4–6). These data add to previous work from our laboratory and others suggesting a critical role for this signaling pathway in neuroblast differentiation (12, 49, 61–65). These studies urge caution in the clinical use of nonspecific tyrosine kinase inhibitors, which may inhibit this important differentiation pathway and lead to disease recurrence.

The increase we observed in serum FGF2 above control levels in a patient subset with improved prognosis suggests that the stroma in these tumors can release ligand to alter systemic levels (Figure 5). Serum FGF2 levels could be used as a prognostic biomarker, as well as a therapeutic biomarker, to select patients for ODSH therapy.

While some HSPGs, including sTβRIII and nonspecific sHSPG, can suppress neuroblast proliferation rapidly within 24 hours, others such as sSDC3 and sSDC4 take longer to have antiproliferative effects (Figure 7 and Supplemental Figure 8). We observed a similar discrepancy with ODSH and heparin: both were potent differentiating agents over a time course of several days and could suppress xenograft growth, but demonstrated different kinetics

in short-term proliferation assays (Figure 6–9 and Supplemental Figure 8). Saccharide length and variable sulfation may contribute to the observed differences, and future studies will investigate the mechanism of delayed effects in some HSPGs and heparin derivatives. sHSPGs did not promote differentiation or suppress proliferation as strongly as did heparin or all-trans retinoic acid (ATRA), suggesting a weaker effect that requires longer treatment (Figure 7 and Supplemental Figures 7 and 8). The consistency we observed between differentiation and proliferation assays supports our conclusion that heparin growth suppression was due to its differentiating effects. During differentiation, neurite outgrowth and Western blot markers increased with distinct kinetics, likely due to differences in the sensitivity of our measurements for these separate biologic processes.

We began our xenograft studies using 1 mg/mouse/day of heparin, in line with previous reports in healthy mice (52, 66, 67). After several instances of fatal anticoagulation in a pilot trial of tumor-bearing mice, we lowered the treatment dose to 0.25 mg/mouse/day. The enhanced sensitivity to heparin anticoagulation in mice bearing orthotopic neuroblastoma xenografts could be due to aberrant tumor vasculature or suppressed drug clearance. These challenges in heparin dosing emphasize the need for development of differentiating strategies that avoid anticoagulation. Indeed, ODSH was well tolerated at the original dose of 1 mg/mouse/day.

In conclusion, we have identified novel roles for HSPGs in neuroblastoma pathogenesis and stroma biology, which led to the discovery of heparin derivatives as differentiating agents with potential clinical utility.

Methods

Microarray dataset analysis. Our microarray meta-dataset was generated as described previously (12). We then queried our meta-dataset using the gene probes listed in Supplemental Table 3. Data for syndecan 4 (SDC4) are from the 3 U133 Plus datasets only, as the Human Exon 1.0 ST Arrays lacked a SDC4 probe. Stromal expression analysis was carried out using the publicly available Albino (31) dataset (GSE7529). This dataset was RMA preprocessed, and all data were $\log_2$ transformed. Survival analysis was conducted using the oncogenomics website (http://home.ccr.cancer.gov/oncology/oncogenomics/), specifically the Oberthuer (34), neuroblastoma prognosis (35), and Seeger (68) datasets. These datasets are denoted herein with roman numerals I, II, and III, respectively. For a list of nonstandard abbreviations and pharmaceuticals, see Supplemental Table 4.

TβRIII, glypican, syndecan, and FGF2 IHC, immunofluorescence, and serum ELISA. Neuroblastoma tissue and serum samples were obtained from the Children's Oncology Group Biorepository with approval from the Neuroblastoma Biology Subcommittee. Remnant pediatric serum samples used as controls were purchased from Bioreclamation LLC. We included 5 control samples from patients under the age of 1 year and 5 samples from patients aged 5 to 11 years. TβRIII, syndecan, and FGF2 IHC was conducted according to the manufacturer's instructions using a previously described biotin-free protocol from BioCare Medical (12). TβRIII was detected using a custom-made rabbit antibody against the cytoplasmic domain and a purified pre-bleed rabbit control, as described previously (12, 69). SDC3 (9496) and SDC4 (15350) antibodies were purchased from Santa Cruz Biotechnology Inc. FGF2 was detected with an antibody (106245) from Abcam. TβRIII, syndecan, and FGF2 IHC was quantified using the ImageJ plugin RGB Measure. Integrated density from the red channel (red stain for the protein of interest) was divided by integrated density from the green channel (methyl green nuclear stain) for early- and late-stage tumor images. This ratio was also determined for a control image (pre-bleed rabbit control stain) of the same stage of neuroblastoma and subtracted from the initial ratio. Early-stage images were compared with late-stage images and are displayed as a percentage (Figure 1B, Figure 5A, and Supplemental Figure 1B). Glypican IHC was performed using heat-induced epitope retrieval (microwaved for 20 minutes in sodium citrate at pH 6.0) and an avidin-biotin–based protocol (69) with antibodies from Sigma-Aldrich (GPC1, no. HPA030571 and GPC3, no. HPA006316), used according to the manufacturer's instructions.

Tissue immunofluorescence was performed as described previously (70, 71) using the IHC antibodies referenced above and the S100 Schwann cell marker antibody (4066) from Abcam.

Multiplex ELISA assays for FGF2 were performed in a 96-well format according to the SearchLight manufacturer's protocol (model 85-5023; Aushon BioSystems). Briefly, diluted samples and standards were incubated at room temperature for 1 hour while shaking using a Labline Titer Plate Shaker (model 4625; Labline Instruments). Plates were washed 3 times using an automated plate washer (ELx405; BioTek Instruments), the biotinylated secondary antibody was added, and the plates were incubated for an additional 30 minutes. After 3 more washes, streptavidin-HRP was added to the plates, and the plates were incubated for 30 minutes, washed again, and SuperSignal substrate was added. Images of the plates were taken within 10 minutes, followed by image analysis using SearchLight Array Analyst software, version 2.1. Analyte concentrations were calculated based on a standard curve derived by performing 4 serial dilutions of the corresponding protein standard on each plate. Patient samples were tested in duplicate, and the mean value was used for analysis.

For the TβRIII ELISA assays, capture antibody (AF-242-PB; R&D Systems) was immobilized onto a Meso Scale Discovery (MSD) MULTI-ARRAY 96-well plate (L15XA-3) overnight at 4°C. The plates were washed, samples were loaded, and the plates were incubated at room temperature for 2 hours while shaking. Detection antibody (BAF-242; R&D Systems) coincubated with streptavidin-SULFO-TAG (R32AD-1; MSD) secondary antibody was applied, and the plates were incubated for 2 hours while shaking and then washed, followed by the addition of MSD Read Buffer T (R92TC-3). Images of the plates were taken within 10 minutes using the MSD Sector Imager 2400, followed by image analysis using MSD Sector Imager software, version 3.0. Analyte concentrations were calculated based on a standard curve derived by performing 6 serial dilutions of the corresponding protein standard on each plate. Patient samples were tested in duplicate, and the mean value was used for analysis.

For the Syndecan-3 ELISA assays, Syndecan-3 DuoSet ELISA capture antibody (DY3539; R&D Systems) was immobilized onto an MSD MULTI-ARRAY 96-well plate (L15XA-3) overnight at 4°C. The plates were washed, samples were loaded, and the plates were incubated at room temperature for 2 hours while shaking. Syndecan-3 DuoSet ELISA detection antibody (DY3539; R&D Systems) coincubated with streptavidin-SULFO-TAG (R32AD-1; MSD) secondary antibody was applied, and the plates were incubated for 2 hours while shaking and were then washed, followed by the addition of MSD Read Buffer T (R92TC-3). Images of the plates were taken within 10 minutes using the MSD Sector Imager 2400, followed by image analysis using MSD Sector Imager software, version 3.0. Analyte concentrations were calculated based on a standard curve derived by performing 6 serial dilutions of the corresponding protein standard on each plate. Patient samples were tested in duplicate, and the mean value was used for analysis.

Commercial ELISA kits were used to measure Human Glypican-1 (MBS920206; MyBioSource) according to the manufacturer's instructions. Sample processing prior to analysis was identical to multiplex sample processing.

Cell culture and reagents. SK-N-SH-SY5Y (5Y; CRL-2266), SK-N-BE (2) (BE2; CRL-2271), SK-N-AS (SK-N-AS; ATCC CRL-2137), DMS53 (CRL-2062), and S16 (ATCC CRL-2941) cells were purchased from ATCC. 5Y and BE2 were grown in a 1:1 mixture of MEM and Ham's F12 with 10% FBS. SK-N-SH-SHEP (SHEP; gift of M.A. Armstrong, Duke University), SK-N-AS, and S16 were grown in DMEM with 10% FBS. DMS53 were grown in Waymouth's MB752/1 with 10% FBS. A549, 293T, COS7, MCF10A, and MDA-MB-231 were sourced and grown as described previously (69, 72, 73). All cells were grown at 37°C in 5% CO_2. Human basic fibroblast growth factor (no. 8910) and the MEK1/2 inhibitor UO126 (no. 9903) were purchased from Cell Signaling Technology. The MEK1/2 inhibitor CI-1040 (no. S1020) was purchased from Selleck Chemicals. The FGFR inhibitor SU5402 (no. 204308) was purchased from Santa Cruz Biotechnology Inc. The FGFR inhibitor PD-173074 (no. P2499) was purchased from Sigma-Aldrich. The neutralizing FGF2 antibody (no. 05-117) was purchased from Millipore and used at a concentration of 5 μg/ml according to the manufacturer's instructions. TAPI2 was purchased from Millipore (no. 579052). Recombinant soluble human TβRIII (no. 242-R3), GPC1 (no. 4519-GP), GPC3 (no. 2119-GP), SDC3 (no. 3539-SD), and SDC4 (no. 2918-SD) were purchased from R&D Systems. HSPG isolated from the basement membrane of Engelbreth-Holm-Swarm mouse sarcoma cells (H4777), retinoic acid p-hydroxyanilide (4-HPR, fenretinide H7779), ATRA (no. R2625), and heparin sodium salt from porcine intestinal mucosa (no. H3149) were purchased from Sigma-Aldrich. The following selectively desulfated heparins were purchased from Iduron Ltd: 2DES (DSH001/2), 6DES (DSH002/6), and NDES (DSH003/N). ODSH was provided by Cantex Pharmaceuticals (formerly ParinGenix Inc.). Coculture experiments used restrictive 0.4 μM Transwells in 12-well dishes (Corning Inc.).

DNA constructs, shRNA/siRNA. All TβRIII and TβRIII shRNA constructs used in this study have been described previously (12). TβRIII-ΔGAG consists of TβRIII-HA with serine-to-alanine point mutations at amino acids 534 and 545 to prevent GAG attachment (12, 47). sTβRIII consists of TβRIII-HA with a truncation at amino acid 781 at the junction with the cytoplasmic domain. sTβRIII S534A was generated using site-directed mutagenesis (Agilent Technologies) of sTβRIII and the same primers as those used to make the 534 serine-to-alanine point mutation in TβRIII-ΔGAG (47). Adenovirus was prepared as described previously (47) and used at an MOI of 10 particles per cell. TβRIII adenoviral shRNA constructs were used at an MOI of 50 particles per cell. Lentiviral vectors consisted of the same construct as those used in adenoviral vectors cloned into a pSMPUW-Neo backbone (TβRIII constructs) or a pLKO.1-puro backbone (TβRIII shRNA construct and nontargeted control). The DNA constructs for GPC3 and sGPC3 (lacking the GPI membrane anchor) were gifts of Jorge Filmus (University of Toronto, Toronto, Ontario, Canada) (74). Transient DNA transfections were performed using Lipofectamine (Invitrogen) according to the manufacturer's instructions.

SDC3 shRNA (no. 41047) and control shRNA (no. 108080) were purchased from Santa Cruz Biotechnology Inc. and used according to the manufacturer's instructions. FGF2 (no. 0000003329) and FGFR1 (no. 0000121102) shRNA knockdown constructs (Mission TRC1; Sigma-Aldrich) were purchased from the Duke University RNAi core facility. pWZL Neo Myr Flag FGFR1 (Addgene plasmid no. 20486) was a gift of Jean Zhao and William Hahn (Dana-Farber Cancer Institute, Boston, Massachusetts, USA) (75). The dominant negative FGFR1 plasmid with a GFP reporter (pCCALL2 dominant negative FGFR1 IRES EGFP) was a gift of Margaret Kirby and Harriett Stadt (Duke University) (76). GPC1 overexpression and shRNA-knockdown adenovirus constructs in the pAd vector were a gift of Andreas Friedl (University of Wisconsin, Madison, Wisconsin, USA) (77). Adenoviruses were generated as described previously (47) and used at an MOI of 10 particles per cell for GPC1 overexpression and 25 particles per cell for GPC1 shRNA knockdown.

Neurite outgrowth analysis. Neurites were measured from phase-contrast images taken with a Nikon inverted microscope at ×10 magnification using the ImageJ plugin NeuronJ (78). Three images were taken of each condition at each time point, and all visible neurites (thin shafts extending outward from the cell body) were measured (70–150 neurites/field).

Western blot analysis. Western blotting was performed as described previously using standard techniques (12). Each experiment was conducted at least 3 times. The following antibodies for differentiation and signaling markers were purchased from Cell Signaling Technology: NF160 (no. 2838), β3-tubulin (no. 5568), TH (no. 2792), NSE (no. 9536), phospho-ERK1/2 (p-ERK1/2) T202/Y204 (no. 9101), ERK1/2 (p-ERK, no. 4695), p21 (no. 2946), p-p38 (no. 4511), p38 (no. 9212), p-AKT (no. 4058), AKT (no. 4691), p-STAT3 (no. 9145), STAT3 (9139), p-SMAD1 (Ser463/465)/SMAD5 (Ser463/465)/SMAD8 (Ser426/428) (no. 9511), SMAD1 (no. 9743), p-SMAD3 (Ser423/425; no. 9520), SMAD3 (no. 9523), and FGFR1 (no. 3471). The β-actin (no. 47778), ID1 (no. sc488), GPC3 (no. 65443), SDC3 (no. 9496), and SDC4 (no. 15350) Western antibodies were purchased from Santa Cruz Biotechnology Inc. The FGF2 (no. 106245) and p-FGFR1 (Y654; no. 9194) Western antibodies were purchased from Abcam.

Iodinated TGF-β1 (NEX2670; PerkinElmer) binding and crosslinking were conducted with TβRIII pulldown using a goat antibody against the extracellular domain (AF-242-PB; R&D Systems) in order to identify functional surface receptor expression, as described previously (69).

Proliferation assays. Tritiated thymidine incorporation was used to assess cell proliferation as described previously (12). Proliferation indices (normalized to control = 1.0) were calculated and averaged for each of 3 individual experiments. Cells were plated in a 96-well plate at a concentration of 5,000 cells per well or 3,000 cells per well (A549, DMS53). Each condition was plated in triplicate overnight prior to a 4-hour [3H]thymidine pulse (1 μCi; Amersham Biosciences, GE Healthcare). Cells were washed with PBS and 5% trichloroacetic acid prior to lysis with 0.1 N NaOH. Incorporation of [3H]thymidine was determined by scintillation counting.

Orthotopic xenograft. The pcDH CMV luciferase EFI Puro vector was a gift of Christine Eyler (Brigham and Women's Hospital, Boston, Massachusetts, USA) (79). After lentiviral transduction and puromycin selection, luciferase expression was confirmed using the IVIS 100 imaging system (Caliper Life Sciences, PerkinElmer). BE2 and SK-N-AS luciferase cell lines were implanted orthotopically (2 million cells/mouse in 15 μl of DMEM) in the left adrenal capsule of 5-week-old female Beige/SCID mice (Charles River Laboratories) as described previously (12). Mice were housed under pathogen-free conditions on a 12-hour light/12-hour dark cycle. Animals were monitored closely for tumor growth and signs of illness and sacrificed at humane endpoints. Heparin (0.25 mg/mouse; H3149; Sigma-Aldrich) and ODSH (1 mg/mouse, Cantex Pharmaceuticals) were delivered in 100 μl PBS via daily i.p. injection as described previously (52, 66, 67). Fenretinide was delivered at 20 μg/kg/day diluted in 100 μl PBS via i.p. injection as described previously in an orthotopic model of neuroblastoma using BE2 cells (54). Firefly D-luciferin potassium salt was purchased from Gold Biotechnology (LUCK-1G) and injected i.p. at a concentration of 150 mg luciferin/kg body weight 5 minutes prior to imaging, according to the manufacturer's instructions. Mice were imaged for 2 minutes, and bioluminescence was calculated using LivingImage software (Caliper Life Sciences) and defined as photon flux (photons/s/cm^2/steradian) over a standard-sized oval region of interest encompassing the body of the mouse. Six-micron xenograft tissue sections were processed using H&E (Richard Allen Hematoxylin no. 72711 and Surgipath Eosin no. 01600) or Ki67 (M7240; Dako) staining according to the manufacturer's instructions. Ki67 stain intensity was quantified using ImmunoRatio software as described previously (80).

Statistics. All clinical and xenograft data were analyzed using nonparametric statistics (Kruskal-Wallis global test with Mann-Whitney *U* post-hoc tests) and presented as median, upper, and lower quartiles. Survival curves were analyzed with log-rank statistics. In vitro experiments were analyzed using parametric statistics (ANOVA global test with Bonferroni-corrected 2-tailed Student's *t* tests as post-hoc tests) and presented as the mean ± SEM. In cases in which data were normalized to control, a 1-sample Student's *t* test was used with an expected value of 1 or 100% in order to decrease the likelihood of a type I error. For all experiments, significance was set at $P < 0.05$. Linear regression was performed on selected microarray data, with the slope and *P* value for the line of best fit reported as well as the R^2 value for the relationship. All of the above statistical analyses were conducted with GraphPad Prism software, version 6.0a (GraphPad Software). Multivariate linear regression was performed on selected microarray data using STATA version 11.2, with the *P* value for the line of best fit reported as well as the R^2 and adjusted R^2 values for the relationship.

Study approval. All patient samples were deidentified, and the project was exempted by the Duke University Health System Institutional Review Board (protocol 00034541). All animal procedures were approved by the Institutional Animal Care and Use Committee of Duke University (protocol A278-11-11).

Acknowledgments

We thank Michael Hogarty, the Children's Oncology Group Neuroblastoma Biology Subcommittee, Wendy London, and Evan Plunkett for providing patient tissue and serum samples. We thank Andreas Friedl, Jorge Filmus, Harriett Stadt, Mary Hutson, Margaret Kirby, and Lisa Crose for providing reagents. We thank Lindsey Morgan and Terri Lucas for coordinating our animal facility use, Julie Fuller for tissue processing, and Alok Tewari, Luke Chen, and Lauren Knelson for microarray dataset processing and statistical analysis. We are grateful to Maurlia Upchurch, Elaine Justice, and Tam How for technical assistance and to Cheryl Alles for outstanding clerical assistance. We are also grateful to Mythreye Karthikeyan, Michael Armstrong, Oren Becher, Daniel Wechsler, Dona Chikaraishi, Christopher Kontos, and Julio Ramirez for invaluable mentoring throughout this project. This work was supported in part by NIH grants F30 CA168043 (to E.H. Knelson), R01-CA136786 (to G.C. Blobe), and R01-CA135006 (to G.C. Blobe), as well as by a Reach Award from Alex's Lemonade Stand (to G.C. Blobe).

Received for publication November 14, 2013, and accepted in revised form February 21, 2014.

Address correspondence to: Gerard C. Blobe, Duke University Medical Center, Box 91004, Durham, North Carolina 27708, USA. Phone: 919-668-1352; Fax: 919-681-6906; E-mail: gerard.blobe@duke.edu.

1. National Cancer Institute. Surveillance, Epidemiology and End Results Program. NIH Web site. http://seer.cancer.gov/. Accessed May 13, 2014.
2. Maris JM, Hogarty MD, Bagatell R, Cohn SL. Neuroblastoma. *Lancet*. 2007;369(9579):2106–2120.
3. Matthay KK, Atkinson JB, Stram DO, Selch M, Reynolds CP, Seeger RC. Patterns of relapse after autologous purged bone marrow transplantation for neuroblastoma: a Childrens Cancer Group pilot study. *J Clin Oncol*. 1993;11(11):2226–2233.
4. Shimada H, Ambros IM, Dehner LP, Hata J, Joshi VV, Roald B. Terminology and morphologic criteria of neuroblastic tumors: recommendations by the International Neuroblastoma Pathology Committee. *Cancer*. 1999;86(2):349–363.
5. Kwiatkowski JL, Rutkowski JL, Yamashiro DJ, Tennekoon GI, Brodeur GM. Schwann cell-conditioned medium promotes neuroblastoma survival and differentiation. *Cancer research*. 1998;58(20):4602–4606.
6. Liu S, Tian Y, Chlenski A, Yang Q, Salwen HR, Cohn SL. 'Cross-talk' between Schwannian stroma and neuroblasts promotes neuroblastoma tumor differentiation and inhibits angiogenesis. *Cancer Lett*. 2005;228(1–2):125–131.
7. Matthay KK, et al. Treatment of high-risk neuroblastoma with intensive chemotherapy, radiotherapy, autologous bone marrow transplantation, and 13-cis-retinoic acid. Children's Cancer Group. *N Engl J Med*. 1999;341(16):1165–1173.
8. Matthay KK, et al. Long-term results for children with high-risk neuroblastoma treated on a randomized trial of myeloablative therapy followed by 13-cis-retinoic acid: a children's oncology group study. *J Clin Oncol*. 2009;27(7):1007–1013.
9. Brodeur GM. Neuroblastoma: biological insights into a clinical enigma. *Nat Rev Cancer*. 2003;3(3):203–216.
10. Edsjo A, Holmquist L, Pahlman S. Neuroblastoma as an experimental model for neuronal differentiation and hypoxia-induced tumor cell dedifferentiation. *Semin Cancer Biol*. 2007;17(3):248–256.
11. Maris JM. Recent advances in neuroblastoma. *N Engl J Med*. 2010;362(23):2202–2211.
12. Knelson EH, Gaviglio AL, Tewari AK, Armstrong MB, Mythreye K, Blobe GC. Type III TGF-β receptor promotes FGF2-mediated neuronal differentiation in neuroblastoma. *J Clin Invest*. 2013; 123(11):4786–4798.
13. Chernousov MA, Carey DJ. N-syndecan (syndecan 3) from neonatal rat brain binds basic fibroblast growth factor. *J Biol Chem*. 1993;268(22):16810–16814.
14. Carey DJ. N-syndecan: structure and function of a transmembrane heparan sulfate proteoglycan. *Perspect Dev Neurobiol*. 1996;3(4):331–346.
15. Hienola A, Tumova S, Kulesskiy E, Rauvala H. N-syndecan deficiency impairs neural migration in brain. *J Cell Biol*. 2006;174(4):569–580.
16. Kinnunen T, Kaksonen M, Saarinen J, Kalkkinen N, Peng HB, Rauvala H. Cortactin-Src kinase signaling pathway is involved in N-syndecan-dependent neurite outgrowth. *J Biol Chem*. 1998; 273(17):10702–10708.
17. Akita K, et al. Heparan sulphate proteoglycans interact with neurocan and promote neurite outgrowth from cerebellar granule cells. *Biochem J*. 2004;383(Pt 1):129–138.
18. Rapraeger AC, Krufka A, Olwin BB. Requirement of heparan sulfate for bFGF-mediated fibroblast growth and myoblast differentiation. *Science*. 1991; 252(5013):1705–1708.
19. Yayon A, Klagsbrun M, Esko JD, Leder P, Ornitz DM. Cell surface, heparin-like molecules are required for binding of basic fibroblast growth factor to its high affinity receptor. *Cell*. 1991;64(4):841–848.
20. Lundin L, et al. Selectively desulfated heparin inhibits fibroblast growth factor-induced mitogenicity and angiogenesis. *J Biol Chem*. 2000;275(32):24653–24660.
21. Takeuchi A, et al. Low molecular weight heparin suppresses receptor for advanced glycation end products-mediated expression of malignant phenotype in human fibrosarcoma cells. *Cancer Sci*. 2013;104(6):740–749.
22. Bendas G, Borsig L. Cancer cell adhesion and metastasis: selectins, integrins, and the inhibitory potential of heparins. *Int J Cell Biol*. 2012;2012:676731.
23. Battinelli EM, et al. Anticoagulation inhibits tumor cell mediated release of platelet angiogenic proteins and diminishes platelet angiogenic response. *Blood*. 2014;123(1):101–112.
24. Ostrovsky O, et al. Differential effects of heparin saccharides on the formation of specific fibroblast growth factor (FGF) and FGF receptor complexes. *J Biol Chem*. 2002;277(4):2444–2453.
25. Whitelock JM, Iozzo RV. Heparan sulfate: a complex polymer charged with biological activity. *Chem Rev*. 2005;105(7):2745–2764.
26. Spivak-Kroizman T, et al. Heparin-induced oligomerization of FGF molecules is responsible for FGF receptor dimerization, activation, and cell proliferation. *Cell*. 1994;79(6):1015–1024.
27. Ornitz DM, Yayon A, Flanagan JG, Svahn CM, Levi E, Leder P. Heparin is required for cell-free binding of basic fibroblast growth factor to a soluble receptor and for mitogenesis in whole cells. *Mol Cell Biol*. 1992;12(1):240–247.
28. Iolascon A, et al. Reduced expression of transforming growth factor-β receptor type III in high stage neuroblastomas. *Br J Cancer*. 2000;82(6):1171–1176.
29. Takita J, et al. Gene expression profiling and identification of novel prognostic marker genes in neuroblastoma. *Genes Chromosomes Cancer*. 2004;40(2):120–132.
30. De Preter K, et al. Human fetal neuroblast and neuroblastoma transcriptome analysis confirms neuroblast origin and highlights neuroblastoma candidate genes. *Genome Biol*. 2006;7(9):R84.
31. Albino D, et al. Identification of low intratumoral gene expression heterogeneity in neuroblastic tumors by genome-wide expression analysis and game theory. *Cancer*. 2008;113(6):1412–1422.
32. Acosta S, et al. Identification of tumoral glial precursor cells in neuroblastoma. *Cancer Lett*. 2011; 312(1):73–81.
33. Ross RA, Biedler JL, Spengler BA. A role for distinct cell types in determining malignancy in human neuroblastoma cell lines and tumors. *Cancer Lett*. 2003;197(1–2):35–39.
34. Oberthuer A, et al. Customized oligonucleotide microarray gene expression-based classification of neuroblastoma patients outperforms current clinical risk stratification. *J Clin Oncol*. 2006; 24(31):5070–5078.
35. Wei JS, et al. Prediction of clinical outcome using gene expression profiling and artificial neural networks for patients with neuroblastoma. *Cancer Res*. 2004;64(19):6883–6891.
36. Pahlman S, Ruusala AI, Abrahamsson L, Mattsson ME, Esscher T. Retinoic acid-induced differentiation of cultured human neuroblastoma cells: a comparison with phorbolester-induced differenti-

ation. *Cell Differ*. 1984;14(2):135–144.
37. Kaneko M, Yang W, Matsumoto Y, Watt F, Funa K. Activity of a novel PDGF beta-receptor enhancer during the cell cycle and upon differentiation of neuroblastoma. *Exp Cell Res*. 2006;312(11):2028–2039.
38. Scarpa S, et al. Transforming growth factor beta regulates differentiation and proliferation of human neuroblastoma. *Exp Cell Res*. 1996;229(1):147–154.
39. Encinas M, et al. Sequential treatment of SH-SY5Y cells with retinoic acid and brain-derived neurotrophic factor gives rise to fully differentiated, neurotrophic factor-dependent, human neuronlike cells. *J Neurochem*. 2000;75(3):991–1003.
40. Hahn CK, et al. Expression-based screening identifies the combination of histone deacetylase inhibitors and retinoids for neuroblastoma differentiation. *Proc Natl Acad Sci U S A*. 2008;105(28):9751–9756.
41. Leli U, Cataldo A, Shea TB, Nixon RA, Hauser G. Distinct mechanisms of differentiation of SH-SY5Y neuroblastoma cells by protein kinase C activators and inhibitors. *J Neurochem*. 1992;58(4):1191–1198.
42. Voigt A, Hartmann P, Zintl F. Differentiation, proliferation and adhesion of human neuroblastoma cells after treatment with retinoic acid. *Cell Adhes Commun*. 2000;7(5):423–440.
43. Kelsh RN. Sorting out Sox10 functions in neural crest development. *Bioessays*. 2006;28(8):788–798.
44. Gershon TR, Oppenheimer O, Chin SS, Gerald WL. Temporally regulated neural crest transcription factors distinguish neuroectodermal tumors of varying malignancy and differentiation. *Neoplasia*. 2005; 7(6):575–584.
45. Mythreye K, Blobe GC. Proteoglycan signaling co-receptors: roles in cell adhesion, migration and invasion. *Cell Signal*. 2009;21(11):1548–1558.
46. Blair CR, Stone JB, Wells RG. The type III TGF-beta receptor betaglycan transmembrane-cytoplasmic domain fragment is stable after ectodomain cleavage and is a substrate of the intramembrane protease gamma-secretase. *Biochim Biophys Acta*. 2011;1813(2):332–339.
47. Kirkbride KC, Townsend TA, Bruinsma MW, Barnett JV, Blobe GC. Bone morphogenetic proteins signal through the transforming growth factor-β type III receptor. *J Biol Chem*. 2008;283(12):7628–7637.
48. Guillemot F, Zimmer C. From cradle to grave: the multiple roles of fibroblast growth factors in neural development. *Neuron*. 2011;71(4):574–588.
49. Lavenius E, Parrow V, Nanberg E, Pahlman S. Basic FGF and IGF-I promote differentiation of human SH-SY5Y neuroblastoma cells in culture. *Growth Factors*. 1994;10(1):29–39.
50. Singh A, et al. Retinoic acid induces REST degradation and neuronal differentiation by modulating the expression of SCF(β-TRCP) in neuroblastoma cells. *Cancer*. 2011;117(22):5189–5202.
51. Thiele C. Neuroblastoma cell lines. In: Masters J, ed. *Human Cell Culture*. Lancaster, United Kingdom: Kluwer Academic Publishers; 1998:21–53.
52. Rao NV, et al. Low anticoagulant heparin targets multiple sites of inflammation, suppresses heparin-induced thrombocytopenia, and inhibits interaction of RAGE with its ligands. *Am J Physiol Cell Physiol*. 2010;299(1):C97–C110.
53. Villablanca JG, et al. Phase II study of oral capsular 4-hydroxyphenylretinamide (4-HPR/fenretinide) in pediatric patients with refractory or recurrent neuroblastoma: a report from the Children's Oncology Group. *Clin Cancer Res*. 2011;17(21):6858–6866.
54. Karmakar S, Choudhury SR, Banik NL, Ray SK. Combination of N-(4-hydroxyphenyl) retinamide and genistein increased apoptosis in neuroblastoma SK-N-BE2 and SH-SY5Y xenografts. *Neuroscience*. 2009;163(1):286–295.
55. Sidell N. Retinoic acid-induced growth inhibition and morphologic differentiation of human neuroblastoma cells in vitro. *J Natl Cancer Inst*. 1982; 68(4):589–596.
56. Gilbert SF. The neural crest. In: *Developmental Biology*. Sunderland, Massachusetts, USA: Sinauer Associates; 2000.
57. Huang D, et al. Schwann cell-conditioned medium inhibits angiogenesis. *Cancer Res*. 2000; 60(21):5966–5971.
58. Huang D, et al. Schwann cell-conditioned medium inhibits angiogenesis in vitro and in vivo. *Med Pediatr Oncol*. 2000;35(6):590–592.
59. Chlenski A, et al. SPARC is a key Schwannian-derived inhibitor controlling neuroblastoma tumor angiogenesis. *Cancer Res*. 2002;62(24):7357–7363.
60. Crawford SE, et al. Pigment epithelium-derived factor (PEDF) in neuroblastoma: a multifunctional mediator of Schwann cell antitumor activity. *J Cell Sci*. 2001;114(pt 24):4421–4428.
61. Kim MS, et al. Fibroblast growth factor 2 induces differentiation and apoptosis of Askin tumour cells. *J Pathol*. 2004;202(1):103–112.
62. Higgins S, et al. Fibroblast growth factor 2 reactivates G1 checkpoint in SK-N-MC cells via regulation of p21, inhibitor of differentiation genes (Id1-3), and epithelium-mesenchyme transition-like events. *Endocrinology*. 2009;150(9):4044–4055.
63. Passiatore G, Gentilella A, Rom S, Pacifici M, Bergonzini V, Peruzzi F. Induction of Id-1 by FGF-2 involves activity of EGR-1 and sensitizes neuroblastoma cells to cell death. *J Cell Physiol*. 2011; 226(7):1763–1770.
64. Wang X, et al. Essential role of ERK activation in neurite outgrowth induced by alpha-lipoic acid. *Biochim Biophys Acta*. 2011;1813(5):827–838.
65. Qiao J, et al. PI3K/AKT and ERK regulate retinoic acid-induced neuroblastoma cellular differentiation. *Biochem Biophys Res Commun*. 2012;424(3):421–426.
66. Wang L, Brown JR, Varki A, Esko JD. Heparin's anti-inflammatory effects require glucosamine 6-O-sulfation and are mediated by blockade of L- and P-selectins. *J Clin Invest*. 2002;110(1):127–136.
67. Myint KM, et al. RAGE control of diabetic nephropathy in a mouse model: effects of RAGE gene disruption and administration of low-molecular weight heparin. *Diabetes*. 2006;55(9):2510–2522.
68. Asgharzadeh S, et al. Prognostic significance of gene expression profiles of metastatic neuroblastomas lacking MYCN gene amplification. *J Natl Cancer Inst*. 2006;98(17):1193–1203.
69. Dong M, et al. The type III TGF-beta receptor suppresses breast cancer progression. *J Clin Invest*. 2007; 117(1):206–217.
70. Mythreye K, Knelson EH, Gatza CE, Gatza Ml, Blobe GC. TβRIII/β-arrestin2 regulates integrin α5β1 trafficking, function, and localization in epithelial cells. *Oncogene*. 2013;32(11):1416–1427.
71. Robertson D, Savage K, Reis-Filho JS, Isacke CM. Multiple immunofluorescence labelling of formalin-fixed paraffin-embedded (FFPE) tissue. *BMC Cell Biol*. 2008;9:13.
72. Finger EC, Turley RS, Dong M, How T, Fields TA, Blobe GC. TβRIII suppresses non-small cell lung cancer invasiveness and tumorigenicity. *Carcinogenesis*. 2008;29(3):528–535.
73. Hanks BA, et al. Type III TGF-β receptor downregulation generates an immunotolerant tumor microenvironment. *J Clin Invest*. 2013;123(9):3925–3940.
74. Zittermann SI, Capurro MI, Shi W, Filmus J. Soluble glypican 3 inhibits the growth of hepatocellular carcinoma in vitro and in vivo. *Int J Cancer*. 2010; 126(6):1291–1301.
75. Boehm JS, et al. Integrative genomic approaches identify IKBKE as a breast cancer oncogene. *Cell*. 2007;129(6):1065–1079.
76. Sato A, et al. FGF8 signaling is chemotactic for cardiac neural crest cells. *Dev Biol*. 2011;354(1):18–30.
77. Qiao D, Yang X, Meyer K, Friedl A. Glypican-1 regulates anaphase promoting complex/cyclosome substrates and cell cycle progression in endothelial cells. *Mol Biol Cell*. 2008;19(7):2789–2801.
78. Meijering E, Jacob M, Sarria JC, Steiner P, Hirling H, Unser M. Design and validation of a tool for neurite tracing and analysis in fluorescence microscopy images. *Cytometry A*. 2004;58(2):167–176.
79. Eyler CE, et al. Glioma stem cell proliferation and tumor growth are promoted by nitric oxide synthase-2. *Cell*. 2011;146(1):53–66.
80. Tuominen VJ, Ruotoistenmaki S, Viitanen A, Jumppanen M, Isola J. ImmunoRatio: a publicly available web application for quantitative image analysis of estrogen receptor (ER), progesterone receptor (PR), and Ki-67. *Breast Cancer Res*. 2010;12(4):R56.